6. HIGHLIGHTS OF LABORATORY FOR ATMOSPHERES ACTIVITIES IN 2000

What sort of results do we get from our work? In this section, you'll learn about the Laboratory's accomplishments for 2000. We have divided this material into two groups. First, you'll see a branch-by-branch summary of highlights. Then, you'll see short articles presenting the results of specific science research highlights.

Summary of Branch Highlights

Data Assimilation Office (DAO), Code 910.3

The Data Assimilation Office (DAO) works to advance the state of the art of data assimilation. The DAO's objectives are:

- To produce research-quality assimilated data sets for addressing questions in studies of the Earth system and of global change
- To make the best use of satellite data for climate assessment
- To assist Earth Observing System science and instrument teams

The DAO's accomplishments in 2000 include—

1) The DAO made major upgrades to the global data assimilation system in use (GEOS), including development of a new version of the core atmospheric circulation model. The upgrades included the following:
   - A revised software architecture (enabling a tropospheric configuration of 1^0x 1^0 and 48 levels, and a stratospheric configuration of 2^0x 2.5^0 and 70 levels)
   - A revised hydrodynamics core
   - Advanced parameterizations of physical processes.

   The latter involved a relaxed Arakawa-Schubert convective scheme, a Mellor-Yamada-type moist-turbulence parameterization, the land-surface model of Koster and Suarez, the long-wave and short-wave radiation scheme of Chou and Suarez, and orographic gravity-wave drag from Zhou et al. A particularly important aspect of GEOS is the physical-space statistical analysis system that provides a global analysis with minimal data selection questions in grid-point space (equivalent to a 3DVAR scheme). Other features are interactive quality control, adaptive estimation of forecast error variance statistics, and non-separable forecast error correlation functions. The interactive quality control of observations enables extreme events to be better captured, with a demonstrable impact from data that would otherwise be rejected. On-line forecast bias correction yields unbiased analyses (especially important for instrument teams). A rapid update cycle (one hour), employed experimentally, improves usage of all asynoptic data, eliminates a spurious tidal signal from analyses and is expected to improve the representation of the hydrological cycle in general. This rapid update cycle is a cost-free partial alternative to 4DVAR.

   The DAO developed two main advances for the GEOS system:

   - A first-look analysis, providing operational support to Mission to Earth Science Enterprise Satellites, especially Terra; e.g., for developing instrument retrieval algorithms

- Final platform analyses using the same information as the first-look analyses together with additional data from Mission to Planet Earth platforms (expected to change as the assimilation system and data availability from the platforms evolve).

2) The DAO further analyzed the impact of including or excluding specific data sets. This analysis has led to significant improvements in the representation of the hydrological cycle and atmospheric energetic terms in the GEOS analyses resulting from the assimilation of TMI and SSM/I rain-rates, as well as total precipitable water. These improvements have resulted in better cloud, moisture, and latent heating distributions in the tropics, and consequently reduced biases in radiative fluxes. Synoptic features were also better represented, and improved forecasts of tropical precipitation (beyond one day) and five-day forecasts generally in the tropics were obtained from the analyzed states. Initial tests using data from QuikSCAT have shown great potential: this is a further example of the major role that can be played by data assimilation in the use, retrieval, and full exploitation of all types of remotely sensed data.

Mesoscale Atmospheric Processes Branch, Code 912

The Mesoscale Atmospheric Processes Branch seeks to understand the contributions of mesoscale atmospheric processes to the global climate system. The Branch studies the physical and dynamical structure and evolution of a broad range of meteorological phenomena ranging from the synoptic scale down to micrometeorology. Branch research focuses on the initiation, development, and effects of cloud systems, such as storms and other climatically significant cloud forms. The major emphasis is on energy exchange and conversion mechanisms associated with turbulence, convection, cloud-scale, mesoscale, and regional-scale phenomena. The work is inherently focused on defining atmospheric components of the global hydrologic cycle and understanding their interaction with other components of the Earth system.

The Branch's accomplishments in 2000 include—

1) Branch scientists derived global precipitation data using satellite observations from the Tropical Rainfall Measurement Mission (TRMM) and earlier and continuing SSM/I and GOES observations, rain gauge networks, and ground-based radar. Branch scientists are heavily engaged in all phases of fieldwork, supporting validation of satellite-derived precipitation estimates including application of an airborne (NASA ER-2) Doppler precipitation radar (EDOP). The Branch is also strongly engaged in future missions such as the AMSR-E on EOS Aqua, to be launched in 2001, and the developing Global Precipitation Mission (GPM).

   A major effort has been made to characterize the rainfall data products generated by different instruments on the TRMM satellite. Data products generated by the passive microwave (TMI) and the active precipitation radar (PR) sensor have been rigorously compared over the globe for the 2.5-year record. This analysis is a key step toward a best estimate of precipitation climatology; i.e., algorithm characterization and improvement and ultimately uniform optimal reprocessing of the data over the mission life.

The spatial and temporal distribution of rainfall over the Amazon basin has been derived from 30-minute 4-km GOES infrared observations calibrated against retrievals from the TRMM Microwave Imager on TRMM. This calibration has enabled the Branch to characterize the diurnal cycle of rainfall, its spatial distribution in response to heterogeneous surface conditions, and the nature of the rainfall (convective versus stratiform).

2) The Branch is active in making measurements of mesoscale and cloud-system structure and processes. Branch members are heavily engaged in developing lidar technology. Lidars allow us to measure an array of atmospheric characteristics at fine temporal and spatial resolution, from airborne platforms, from satellite platforms, and from the ground. For instance, the Cloud Physics Lidar (CPL) characterizes the profile structure of cloud systems. The Micro Pulse Lidar (MPL), the Large Aperture Scanning Airborne Lidar (LASAL), and most other lidar systems enable us to measure atmospheric aerosols. The Scanning Raman Lidar (SRL) and Raman Airborne Spectroscopic Lidar (RASL) allow us to characterize water vapor. Finally, the Goddard Lidar Observatory for Winds (GLOW) enables us to characterize winds. Of particular note are capabilities to characterize atmospheric structure in the planetary boundary layer and in upper tropospheric cirrus clouds. A key activity is the central role played by Branch scientists in the development of the atmosphere-sensing capabilities of the GLAS system that will be launched on ICEsat late in 2001. Branch scientists are also involved in the PICASSO-CENA (lidar) and CloudSat (mm-radar) missions that are planned for launch in 2003.

   A major accomplishment was the rapid development and integration of the Cloud Physics Lidar, successor to Cloud Lidar System, for flights on the NASA ER-2. This new and greatly improved instrument incorporates recent technology advances to facilitate improved sensing capabilities and data products at reduced size and weight. The CPL permits vastly more rapid production of calibrated science-quality data sets (days versus months). The system was deployed to the SAFARI-2000 field experiment, a major international experiment and a core validation activity for the EOS Terra mission. CPL captured valuable data sets characterizing the complex layered structure of aerosol within the southern African gyre. CPL has already assumed its role as a key airborne sensor for studies of aerosols and cloud systems, especially in development and validation of algorithms for application to present and future satellite-based measurements.

   Another highlight was the successful field tests of the Holographic Airborne Rotating Lidar Instrument Experiment (HARLIE). The mechanical simplicity and high fidelity of this new lightweight "telescope" technology has great promise in future lidar-based remote-sensing.

3) The Branch is active in modeling mesoscale cloud systems. Atmospheric dynamics models represent our best understanding of atmospheric processes and provide the capability of studying these processes and their interactions in ways not possible with observations, e.g., establishing cause and effect. A suite of overlapping cloud-system models has been developed that spans a range of scales and processes. The suite includes a state-of-the-art mesoscale model (MM5) that allows regional studies of weather systems at sub-synoptic scales, a cloud system model (GCE) that allows high-resolution studies of cloud systems with special emphasis on precipitating deep convective clouds, and very-high-resolution cirrus cloud models. These models can be coupled to a comprehensive land-surface (vegetation) model and an ocean model to study the interactions of surface processes with the overlying atmosphere.

The Branch has produced high-resolution simulations of hurricanes with MM5, using a spectrum of boundary-layer parameterizations to establish the strong sensitivity of hurricane intensity and structure to surface fluxes. Detailed analysis indicates that horizontal eddy transports into the eye region play a key role in storm intensification and precipitation structure, in agreement with recent theoretical arguments.

Branch study of convective triggering and the role of land-surface heterogeneity indicate that cumulus parameterizations should be applied over multiple individual landscape patches within a GCM grid box, rather than to the grid box as a whole, as occurs in present climate system models.

Branch scientists actively participate in and lead international model comparison and evaluation activities of the GEWEX Cloud System Study. These activities aim to increase confidence in these tools and facilitate research on the development and testing of cloud parameterizations used in large-scale climate and forecast models (GCMs).

The Branch has developed a visualization lab and Electronic Theater that is being increasingly used in high-profile settings to reach out to scientists and, importantly, to citizens and government organizations to stimulate understanding and support of NASA's Earth Science Enterprise and its endeavors. The lab's capabilities are heavily employed by the TRMM Outreach Office, a group that has had a remarkable year in bringing the value of TRMM and TRMM-science to the forefront of US global change research. The American Meteorological Society (AMS) includes the Branch's Electronic Theater in all its annual meetings.

Climate and Radiation Branch, Code 913

The Climate and Radiation Branch conducts research on the causes and consequences of regional and global climate variability. The Branch focuses on underlying physical processes, especially those associated with the formation of aerosols, clouds, and precipitation, and their interaction with atmospheric dynamics and radiation. Research is carried out using a combination of data from space-based as well as ground-based data in parallel with a hierarchy of models from cloud-resolving scales to global system models.

The Branch's accomplishments in 2000 include—

1) Branch scientists use satellite and remote-sensing data to improve our understanding of the physical processes responsible for the formation of clouds, precipitation and their interactions with the water and energy cycles.

They found new evidence of climate sensitivity to global warming based on satellite data that demonstrated decreasing high-level clouds over the tropical western Pacific as the mean sea surface temperature of the cloudy region increases. Branch scientists developed an improved rain retrieval method based on spatial structures of the TRMM microwave radiometer (TMI) observations. The method will provide better discrimination of convective and stratiform precipitation. Branch scientists also developed a simple method of estimating mean squared random error in monthly rainfall estimates, based on quantities that can be directly computed from the satellite data. This method will have potential application in the design of the Global Precipitation Mission (GPM).

2) Branch scientists developed better retrieval techniques for optical and radiative properties of aerosols and clouds to assess their impact on climate change.

   Using preliminary data from Terra, Branch scientists demonstrated for the first time that we can use the combination of aerosol measurements from MODIS and MISR, carbon monoxide measurements from MOPITT, and energy measurements from CERES to distinguish man-made combustion aerosol from natural aerosol. This capability will allow us to identify fingerprints of human impact on climate change. Branch members streamlined the Terra data system to allow the Forest Service to use MODIS images for monitoring the wildfires of August 2000 in Montana and Idaho. This use of Terra data permitted unprecedented near-real-time (within 15 hours) observations of fires, smoke, and the spread of pollution. The Branch also conducted international model-comparison projects that documented significant inter-model differences in the cirrus cloud models used in global climate studies.

3) Branch scientists continued their modeling and diagnostic studies to better understand the mechanisms of climate variations, climate processes, and predictability.

   They demonstrated that remote forcing from radiative cooling in the subsidence region exerts strong control on the cloudiness distribution in the warm pool region, and that the gradient of SST likely plays an important role in controlling cloud radiative feedback associated with global warming. Branch scientists identified the impact of El Niño on the occurrence of regional floods and droughts. Their findings demonstrate that extreme precipitation events over Asia and North America may be connected through climate teleconnections. Branch scientists proposed a new interpretation of monsoon mechanisms based on atmospheric general circulation experiments, developed a new generation catchment-based land-surface model for use in climate studies, carried out experimental dynamical seasonal predictions with a state-of-the-art production version of the NSIPP atmospheric GCM, and developed a new parameterization for snow cover. Their new approach to snow cover included separate predictions of the temperatures of snow and the ground underneath. These advances promise better climate simulations in atmospheric general circulation models.

4) The Branch developed advanced concepts for furthering research and technology into operational programs and projects.

   Branch members championed and submitted a proposal to NASA Headquarters for establishing a Center of Excellence for Aerosol Climate Research within the Laboratory. Branch members also developed a science plan and methodologies to deploy an advanced imaging instrument to retrieve information about the effects of aerosols on cloud reflectivity, for the first Earth-viewing satellite, Triana, at the L-1 point. The Branch conducted an international workshop on "Inter-comparison of 3-dimensional (3D) Radiation Codes" with five goals :

- To understand the errors and limits of 3D methods
- To provide 'baseline' for future 3D code development
- To promote sharing of 3D tools
- To derive guidelines for 3D tool selection
- To improve atmospheric science education in 3D radiation

   Branch members also fabricated a laboratory instrument, the THOR lidar, which is designed to measure cloud thickness from off-beam lidar returns. The instrument is being

prepared for airborne deployment and for competitive award under the Instrument Incubator Program (IIP).

Atmospheric Experiment Branch, Code 915

The Atmospheric Experiment Branch conducts experimental studies to increase our understanding of the chemical environment in our solar system during its formation and to study the physical processes that have continued to shape solar system bodies through time. To achieve this goal, the Branch has a comprehensive program of experimental research, developing instruments to make detailed measurements of the chemical composition of solar system bodies such as comets, planets, and planetary systems that can be reached by space probes or satellites.

The Branch's accomplishments for 2000 include—

1) The Branch continued participation in the CONTOUR mission that will rendezvous with three comets and provide a more detailed understanding of the cometary nuclei and the diversity among comets. Branch members are building a Neutral Gas and Ion Mass Spectrometer (NGIMS) in-house. Scheduled delivery of the instrument is September 2001 with a launch in July 2002. The NGIMS instrument team successfully completed both a preliminary design review and a critical design review during the past year. The instrument design and parts fabrication have been completed and instrument assembly is underway.

2) The Branch continued providing post-launch support for several key planetary missions. These include—

- A Gas Chromatograph Mass Spectrometer on the Cassini Huygens Probe mission to explore the atmosphere of Saturn's moon Titan
- An Ion and Neutral Mass Spectrometer on the Cassini Orbiter to explore the upper atmosphere of both Saturn and Titan
- A Neutral Mass Spectrometer on the Japanese *Nozomi* mission to explore the upper atmosphere of Mars.

  In addition, Branch members continue to refine flight data from the Galileo Probe Neutral Mass Spectrometer.

3) Branch members submitted instrument proposals for two Discovery missions. One mission, the Venus Atmosphere Measurement Probe, entails an entry probe mission to explore the lower atmosphere of Venus. The Branch will provide a mass spectrometer for this mission. The second mission is called Odyssey. Odyssey will rendezvous with the Comet Kopff. The Branch will provide a gas chromatograph mass spectrometer similar to the one that would have flown on the cancelled Champollion mission.

4) An important collaborative effort with GSFC's Engineering Directorate has been initiated during this past year. This collaboration calls for a comprehensive program to achieve a significant reduction in the size and weight of present-day mass spectrometer systems by using MEMS technology. The effort will unfold in two steps: The first step is to use Application Specific Integrated Circuits to reduce the size and weight of the electronics. The second step will use the GSFC in-house skills and facilities to develop a miniaturized MEMS mass spectrometer. This effort will be expanded next year to promote collaboration with universities.

Atmospheric Chemistry and Dynamics Branch, Code 916

The Atmospheric Chemistry and Dynamics Branch conducts research in understanding the distribution and variability of atmospheric ozone by making new measurements, by analysis of existing data, and by theoretically modeling the chemistry and transport of trace gases that control the behavior of ozone. An emerging research focus is the characterization of sources and sinks of aerosols and other atmospheric trace gases that control global air quality.

The Branch's accomplishments for 2000 include—

1) Branch scientists took the lead in organizing and conducting several aircraft and field campaigns, including the recently concluded SOLVE (SAGE III Ozone Loss and Validation Experiment) mission, designed to better understand the causes of ozone loss in the Arctic. Branch scientists provided a key instrument for this mission—the AROTEL lidar—developed in collaboration with Langley Research Center scientists to measure aerosol, ozone, and temperature above the aircraft cruise altitude.

2) Branch scientists have used data from the TRMM and UARS satellites as well as aircraft and balloon measurements to investigate the processes that regulate water vapor in the tropical upper troposphere. We have begun looking at processes occurring at the tropical tropopause that regulate stratospheric humidity. Our goal is to understand how human-induced climate change will affect these processes and, thereby, change the water vapor abundance of the stratosphere.

3) Branch scientists developed new techniques for measuring tropospheric aerosols, clouds, ozone, and air quality using a new generation of space-based instruments. Some of these ideas were incorporated in the scientifically enhanced Triana satellite mission. These enhancements were key factors in the National Academy of Science's decision to endorse the mission. Two ESSP missions based on these ideas are being developed, and more sensitive instruments to measure carbon dioxide from space are in the planning stage. NASA Headquarters selected several Branch scientists as members of the OMI science team to implement these ideas and to lead the 15-member US science team. (OMI is a Netherlands-provided instrument, scheduled to fly on the EOS Aura satellite in the year 2003.)

4) Branch scientists developed a new technique for merging different types of satellite and ground-based data to create a homogeneous long-term record of the total column ozone. This data set will play a key role in the upcoming international assessment of the health of the ozone layer. This congressionally mandated study is due in 2002 and will report on whether the ozone layer has begun to recover in response to decreasing concentrations of CFCs and other ozone-destroying chemicals.

5) Branch scientists developed a new 20-year record of aerosols by improved analysis of TOMS UV reflectance data. This data set is the only global aerosol data over land and the only data that can separate UV-absorbing aerosols (e.g., smoke from biomass burning and mineral dust from the deserts) from other types of aerosols (e.g., sulfates).

6) Branch scientists developed a 20-year record of tropical troposphere column ozone using the TOMS data. This data set has highlighted the importance of tropical oscillations (South-Atlantic Oscillations, also known as El Niño, and the quasi-biennial oscillations in longitudinal winds) in determining the distribution of tropospheric ozone. These natural signals mix with anthropogenic signals from biomass burning over Africa and South America to create a complicated spatial and temporal variability seen in the data record. To improve the understanding of these processes, the Branch scientists organized an international program called SHADOZ (Southern Hemisphere Additional Ozonesondes). This program aims at improving the quality and quantity of ozone vertical profile data in the region of the world that is experiencing rapid environmental change.

Scientific Research Highlights

Now that you've seen general summaries of our Branch accomplishments, let's have a closer look at the results of our research. The following pages present the Laboratory's scientific highlights for 2000, divided into three disciplines: Measurements, Data Analysis, and Modeling. Table IV lists the contents of these three sections.

Table IV: Summary of Scientific Research Highlights

Measurements	Data Analysis	Modeling
Ground-Based Measurements **Surface Measurements for Atmospheric Radiative Transfer (SMART)** Si-Chee Tsay, Code 913 **MPL-Net** James Spinhirne, Code 912 **Field Campaigns** **SAGE III Ozone Loss and Validation Experiment (SOLVE)** Paul A. Newman, Code 916 **Field Campaigns, PRiDE, SAFARI-2000, and ACE-Asia** Si-Chee Tsay, Code 913 **SAVE/SAFARI-2000 Ozonesonde Launches in Lusaka, Zambia** Anne M. Thompson, Code 916 **Airborne ER-2 Cloud Physics Lidar System** Matt McGill, Code 912 **Instrument Development** **Geoscience Laser Altimeter System (GLAS)** James Spinhirne, Code 912 **GSFC Airborne Raman Ozone, Temperature, and Aerosol Lidar (AROTEL)** Thomas J. McGee, Code 916	**Aerosol Studies** **Operational Use of MODIS/Terra Data for Monitoring Fires in Montana and Idaho** Yoram Kaufman, Code 913 **Smoke Aerosol from Biomass Burning in Mexico, Hygroscopic Smoke Optical Model** Lorraine A. Remer, Code 913 **Clouds and Precipitation** **Accuracy of TRMM Monthly Rainfall Maps** Thomas L. Bell, Code 913 **Effect of Radiative Cooling on the Relation between Cloud and Sea Surface Temperature** Chung-Hsiung Sui, Code 913 **The Use of Vegetation for Estimating Broken-Cloud Optical Properties from Surface Radiance Measurements** Alexander Marshak, Code 913 **Effects of Clouds on the Solar Heating of the Atmosphere in the Tropical Western Pacific** Ming-Dah Chou, Code 913 **Climate Variability and Climate Change** **A Multiyear Data Set of SSM/I Derived Global Ocean Surface Turbulent Fluxes** Shu-Hsien Chou, Code 912 **Planetary Sciences** **Galileo Mission Highlights** Paul R. Mahaffy, Code 915	**Data Assimilation** **Improving Four-Dimensional Global Data Sets and Short-Range Forecasts Using TRMM and SSM/I-Derived Rainfall and Moisture Observations** Arthur Hou, Code 910.3 **DAO Supports the SOLVE Mission** Steve Pawson, Code 910.3 **The Predictability of Seasonal Means During Northern Summer** Siegfried Schubert, Code 910.3 **An Analysis of the Madden-Julian Oscillation** Siegfried Schubert, Code 910.3 **GEOS Ozone Data Assimilation System** Lars Peter Riishojgaard, Code 910.3 **Land Temperature Assimilation** Arlindo da Silva, Code 910.3 **Hurricanes** **Numerical Modeling of Hurricanes** Scott Braun, Code 912 **Physical Processes** **Force-Restore Snow Physics in SSiB** Yogesh Sud, Code 913 **Cirrus Cloud Models** David Starr, Code 912

Measurements

Ground-Based Measurements

Surface Measurements for Atmospheric Radiative Transfer (SMART)

Much of the Laboratory's research focuses on the remote sensing and retrieval of physical/radiative properties of Earth's atmosphere (e.g., clouds, aerosols, and molecular constituents) and surface (e.g., soil and vegetation). To capture this data, we are mobilizing an evolving suite of remote-sensing instruments. We call this suite SMART, signifying Surface Measurements for Atmospheric Radiative Transfer. We will combine SMART observations with those from satellite nadir overpasses at targeted areas.

The SMART, as shown in Figure 2, includes broadband radiometers, shadow-band radiometer, sunphotometers, solar spectrometers, a whole-sky camera, a micro-pulse lidar, and a microwave radiometer, as well as meteorological probes for atmospheric pressure, temperature, humidity, and wind speed and direction.

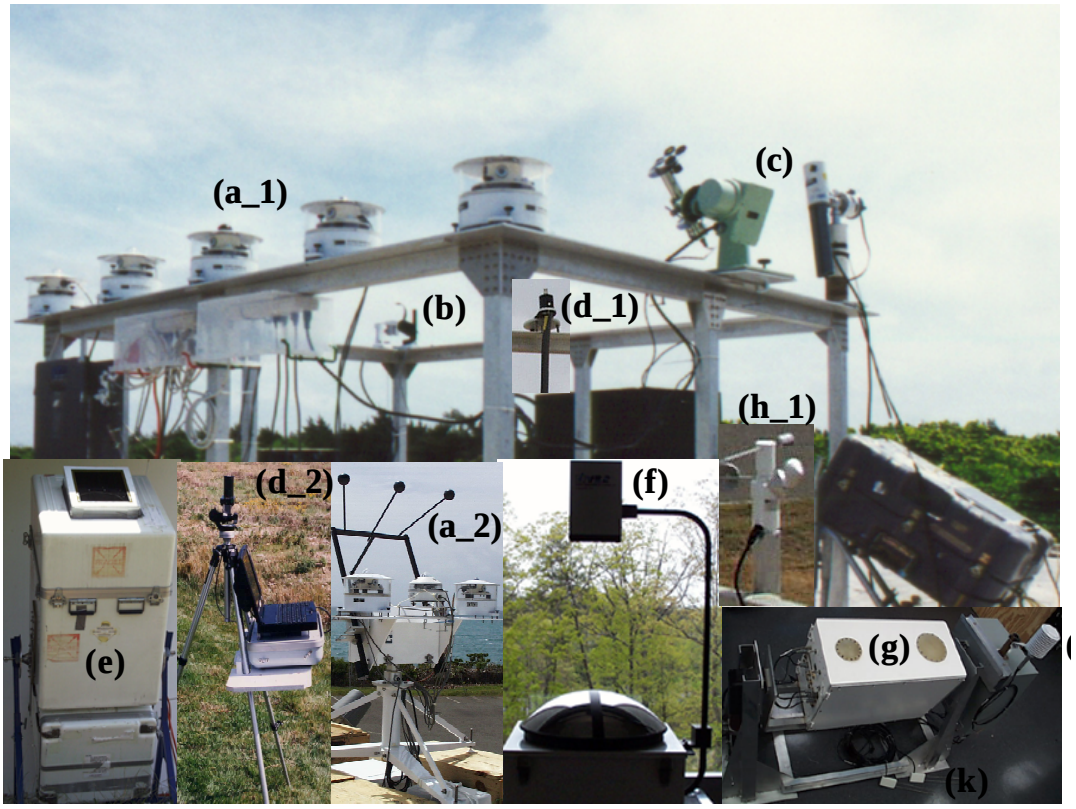

Figure 2. The SMART setup: (a) multiple shortwave longwave broadband radiometers, (b) shadow-band radiometer, (c) sunphotometers, (d) solar spectrometers, (e) micro-pulse lidar, (f) whole-sky camera, and (g) microwave radiometer, as well as (h) meteorological probes for atmospheric pressure, temperature, humidity, wind speed/direction and, surface moisture content (not shown).

During 2000, SMART was successfully deployed to the PRiDE and SAFARI-2000 campaigns. Adding to our instrument development, we have completed the 3S (Sun-Sky-Surface) photometer and LAS (Leonardo Airborne Simulator) spectrometer. The 3S fabrication was funded through GSFC/DDF, with the collaboration of the Biophysics Branch (Code 923) and the Detector System Branch (Code 553). The 3S proved its superiority over the aging Cimel sunphotometer during its deployment on SAFARI-2000 to the AERONET site at Mongu, Zambia. The 3S contains 14 discrete channels, covering from ultraviolet to shortwave-infrared spectral region. It scans the upper (atmosphere) and lower (surface) hemispheres during its operation, as depicted in Figure 3.

Figure 3. Current operation of the 3S photometer, in contrast with the 8-channel, filter-wheeled Cimel sunphotometer in the background.

To prepare for future space formation flights, we collaborated on the fabrication of a compact, low-power, low-cost, Earth-viewing spectrometer. Our partners in this work were scientists D. Reuter of Code 693 and J. Tucker of Code 923, and engineers M. Jhabvala of Code 550 and P. Shu of Code 553. This prototype spectrometer, named the *Leonardo* Airborne Simulator (LAS), flew successfully for the first time in NASA's ER-2 high-altitude aircraft during SAFARI-2000 campaign. Operating in a push broom mode, LAS obtains a 3-D data cube by scanning the image of a surface over the focal plane (one axis of the array for spectral and the other for spatial sampling). The scanning motion is provided by the aircraft trajectory. A state-of-the-art detector, 1024 × 1024 Indium Antimonide array, is used in the LAS focal plane. The detector covers the entire shortwave spectral region (0.4-5.0 μm, typical quantum efficiency >80% everywhere, with proper anti-reflection coating for $\lambda < 1$ μm) thereby avoiding excessive patching-together of spectra. Figure 4 depicts the LAS, consisting of two modules, integrated in the ER-2 research aircraft. LAS records a scene spectrally through a wedged filter (linear variable filter, LVF) placed close to the detector array.

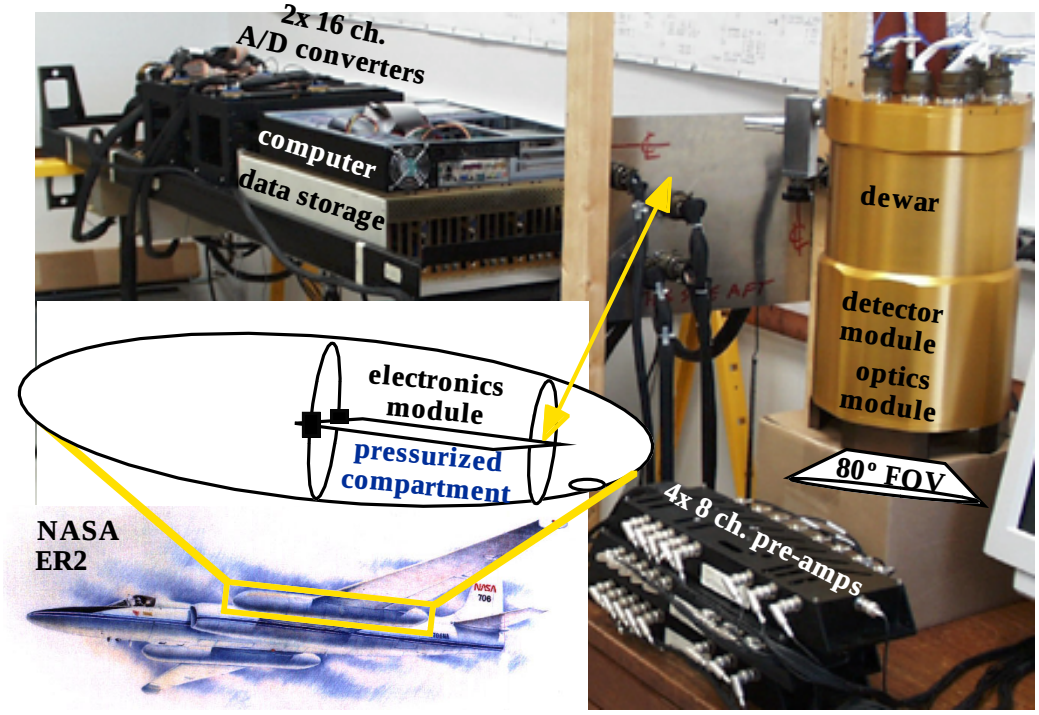

Figure 4. The LAS sensor subsystem (non-pressurized compartment, back portion of ER-2 super pod) contains the focal plane, imaging optics, and those electronics that must be near the detector arrays. Residing in pressurized compartment, the electronics module contains interface electronics that can be farther from the arrays.

In essence, the LVF achieves a spectral resolving power ($\lambda/\Delta\lambda$) of at least 500 (e.g., 1 nm at 0.5 µm and 5 nm at 2.5 µm), with the flexibility of having coarser resolution in some parts of the spectrum and finer resolution in others. The segmented wedged filter as the wavelength selective element on a single focal plane allows for a unique solution to the challenge of obtaining a wide field of view (90° FOV) over a broad wavelength range. Current optimal design of LAS uses the refractive module for simplicity and budgetary concern. This, however, is near the current limit for a single LVF segment in covering wavelength range of 0.4–2.5 µm. In the next stage, a reflective module will be sought to extend the full wavelength coverage with wide field of view, e.g., 120°.

Si-Chee Tsay, Code 913 (Si-Chee.Tsay.1@gsfc.nasa.gov)

MPL – Net

We have begun development of the world's first network of automated, full-time surface lidar observations of clouds and aerosols through a new project now funded by the EOS program. The network consists of micro-pulse lidar systems (MPL), which were developed, patented, and commercialized by the GSFC cloud and aerosol lidar group. The MPL network, named MPL-Net, currently consists of one site at the South Pole, one site at Goddard Space Flight Center, and four sites at Atmospheric Radiation Measurement (ARM) program locations. All MPL-Net sites are co-located with AERONET sunphotometers to acquire joint measurements of cloud and aerosol vertical distributions, optical depth, and sky radiance. Planning is underway for the installation of the next two MPL-Net sites in Saudi Arabia and Barbados. Other sites under consideration include locations in Japan, Korea, Taiwan, and Australia.

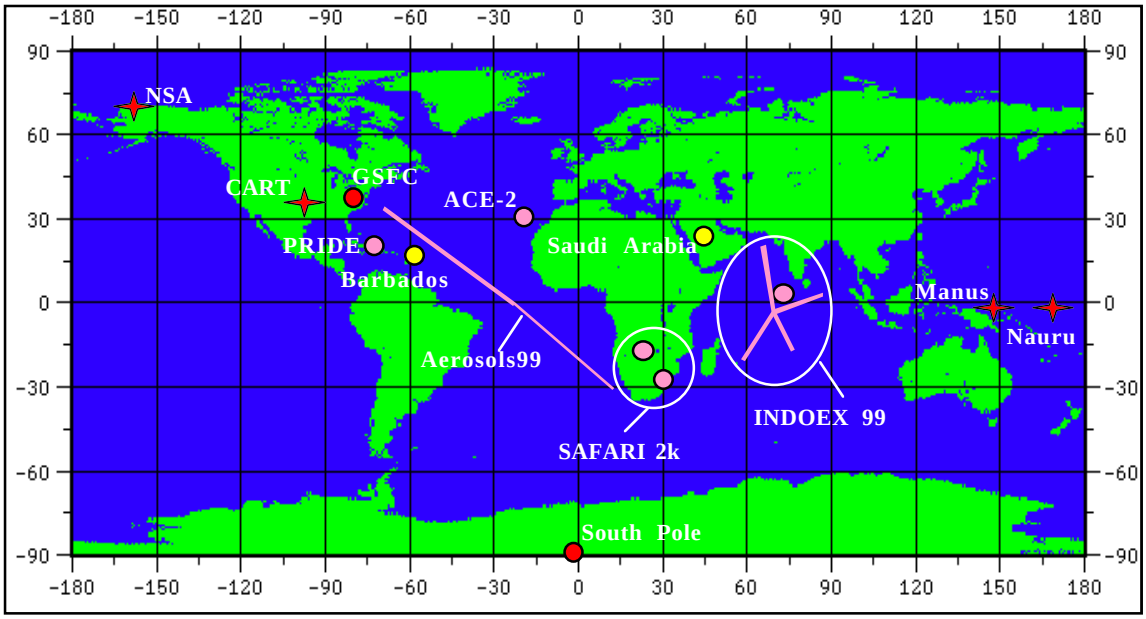

Figure 5. Map of existing and proposed MPL-Net sites. Recent field experiments and ship cruises are also shown. MPL-Net sites/experiments are shown with a circle, ARM sites with a black square, and ship cruises with a line. Existing sites are shown in red, proposed sites in pink, and experiments and cruises in pink.

In addition to the long-term site measurements, MPL-Net provides support for field experiments and ship cruises each year. The field experiments provide for an intensive study of cloud and aerosol properties by combining a variety of different measurement techniques. MPL-Net participated in three field experiments during the year 2000: an ARM cloud experiment in Oklahoma, the Puerto Rico Dust Experiment (PRiDE), and SAFARI-2000 in southern Africa. In the spring of 2001, MPL-Net will participate in the ACE-Asia experiment. During ACE-Asia one MPL will be deployed on board a research vessel and another in China in order to study the transport of Asian dust and pollution as it moves out over the Pacific Ocean.

The observations from MPL-Net will provide a unique data set for understanding the effects of clouds and aerosols on the atmosphere's radiation balance. For more information, see the MPL-Net Web site (http://virl.gsfc.nasa.gov/mpl-net/).

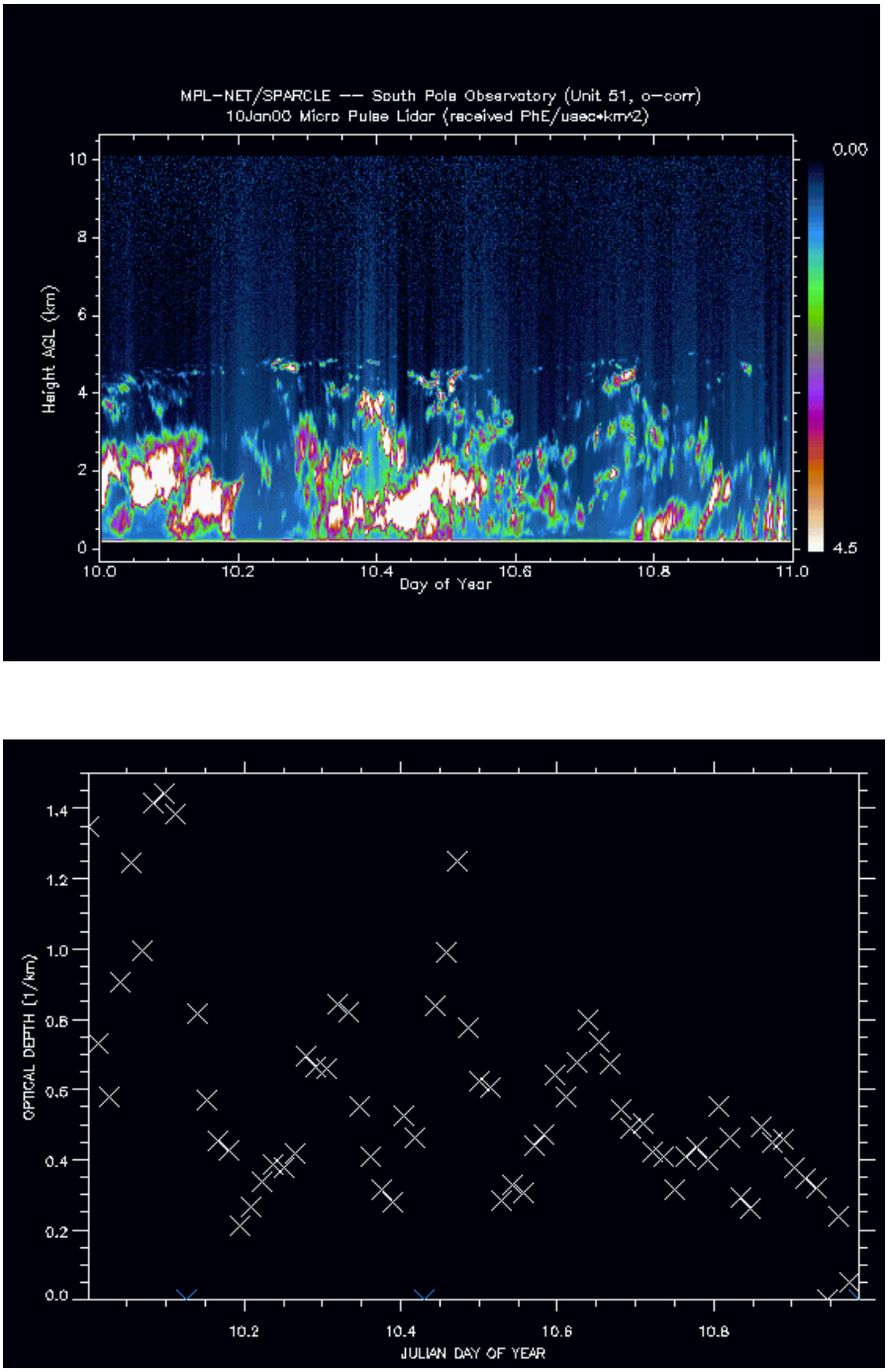

Figure 6. MPL data from the South Pole site on January 10, 2000. The upper graph shows MPL signals during the course of the day. The signal returns are from blowing snow and clouds at the site. The lower graph displays the particulate optical depth from the surface to 6 km. (On clear days the optical depth is near zero.)

James Spinhirne, Code 912 (James.D.Spinhirne.1@gsfc.nasa.gov)

Field Campaigns

SAGE III Ozone Loss and Validation Experiment (SOLVE)

During the winter of 1999-2000, the NASA-sponsored SAGE III Ozone Loss and Validation Experiment (SOLVE) was jointly conducted with the European Commission-sponsored Third European Stratospheric Experiment on Ozone (THESEO-2000).

This SOLVE/THESEO-2000 mission was designed to both investigate the processes that control polar and mid-latitude winter and spring ozone levels, and to validate measurements from the Stratospheric Aerosol and Gas Experiment (SAGE) instrument. Unfortunately, SAGE III was not launched on schedule, but SOLVE/THESEO-2000 was able to take advantage of our other satellite assets to understand polar ozone losses from this last winter.

The 1999-2000 Arctic stratospheric winter was very cold, leading to the appearance of extensive decks of polar stratospheric clouds (PSCs) across the Arctic lower stratosphere. The importance of these PSCs to the chemistry of the stratosphere is that they convert the reservoir species HCl and $ClONO_2$ into reactive forms of chlorine that can destroy ozone. In agreement with this chlorine conversion, extremely high levels of ClO were measured during the spring in the Arctic. These high chlorine levels led to ozone losses of about 60% in a layer near about 20-km altitude over the Arctic.

Although PSCs have been observed in the stratosphere for more than a century, there was actually little information on the particle sizes or composition. Direct observations using the NASA ER-2 and DC-8 aircraft have confirmed that these unique clouds are key components of the ozone loss process. Further, it is now understood how these cloud particles modify the stratosphere as they slowly fall. Such information will be applied in both diagnostic and assessment models for more accurate predictions of changes in stratospheric ozone.

The Laboratory for Atmospheres played a key role in the SOLVE/THESEO-2000 mission. Drs. Paul A. Newman and Mark R. Schoeberl helped develop the overall mission strategy and also served as project scientists for the mission. Forecasts, modeling, and flight planning work was provided by the Atmospheric Chemistry and Dynamics Branch. The Data Assimilation Office provided meteorological analyses and forecasts over the entire course of the mission from November 1999 through March 2000. The AROTEL Lidar system was also provided by the Atmospheric Chemistry and Dynamics Branch for flights on board the NASA DC-8. This lidar system was a joint effort of Drs. Thomas McGee and John Burris in association with Dr. Chris Hostetler of NASA LaRC. The lidar provided crucial information of polar ozone and temperature distributions during all three SOLVE deployments. Figure 7 shows ozone measurements taken during two flights in December 1999 and March 2000. The figure reveals a large decrease of ozone between December and March at an altitude near 18 km. This low ozone region results from catalytic destruction by chlorine and bromine species over the course of the winter and early spring. These chlorine and bromine species principally come from man-made compounds such as chlorofluorocarbons and halons.

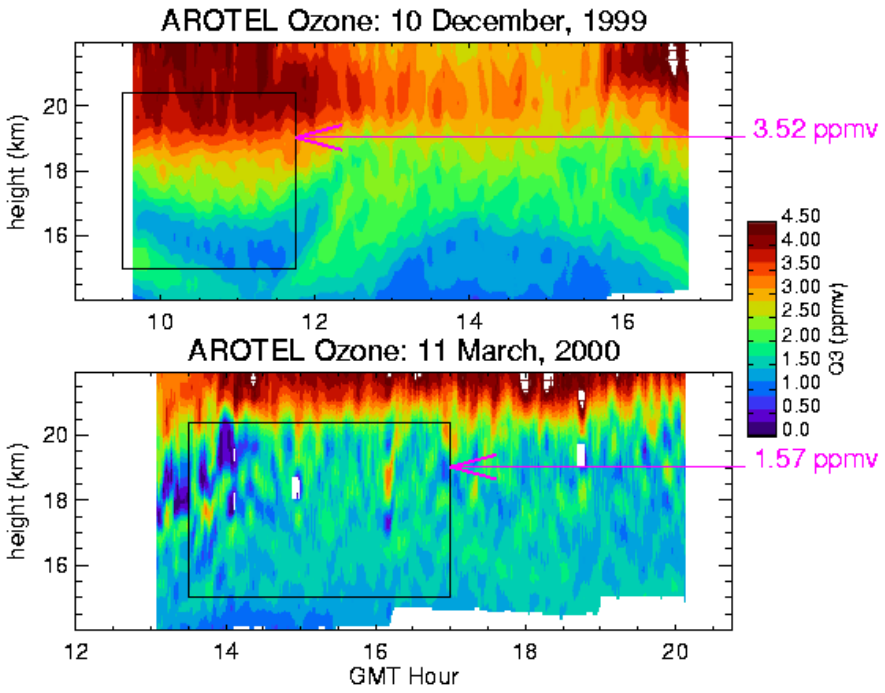

Figure 7. The figure shows ozone measurements taken during two SOLVE DC-8 flights in December 1999 and March 2000. The figures illustrate the large decrease in ozone between December and March at an altitude near 18 km

Paul A. Newman, Code 916 (Paul.A.Newman.1@gsfc.nasa.gov)

Field Campaigns, PRiDE, SAFARI-2000, and ACE-Asia

During 2000, we participated in two major field campaigns, PRiDE (Puerto Rico Dust Experiment) and SAFARI-2000 (Southern Africa Fire-Atmosphere Research Initiative), as part of the EOS science and validation tasks. We are also in the final planning stage for ACE-Asia (Aerosol Characterization Experiment-Asia), to be conducted in 2001. These field research activities are summarized below.

PRiDE, June-July 2000, in the vicinity of Puerto Rico

PRiDE was designed to measure the properties of Saharan dust transported across the Atlantic Ocean to the Caribbean. PRiDE is a collaborative endeavor with the Office of Naval Research and the University of Miami. In the summer months, moderate quantities of desert dust are observed in the Caribbean (cf. Fig. 8). Analyses of NOAA/AVHRR and EOS/AERONET data suggest that in June and July, mid-visible optical depth in the Caribbean can vary from 0.2 to 0.7, with a mean value of ~0.4. Puerto Rico is the first significant landfall for the dust traveling across the ocean from Africa. Other types of man-made aerosol pollutants, which may complicate the analysis, should not affect dust arriving on the eastern end of the island

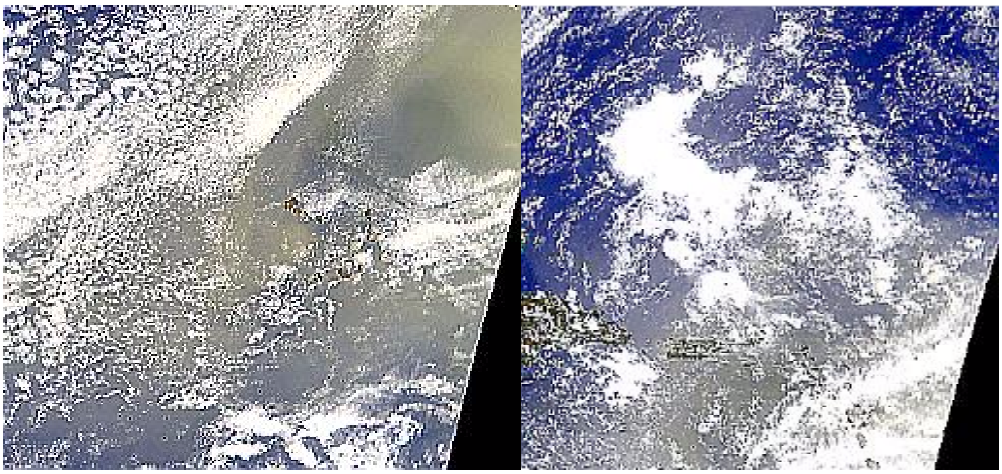

Figure 8. Typical satellite imagery observed by SeaWiFS depicts the Saharan dust outbreak over Cape Verde Island (upper-right quadrant of left image) and transported to the vicinity of Puerto Rico Island (lower half of right image).

During PRiDE, we recorded aerosol optical thickness, precipitable water vapor, and downwelling irradiance. We gathered these measurements with the SMART suite of instruments and from a low-flying aircraft during the MODIS overpass. The data can reveal the extent to which we must know the properties of dust particles and the spectral surface reflectance of the ocean before we can use remote-sensing systems to accurately retrieve optical thickness and radiative flux. We will compare these ground-based observations with the MODIS retrievals over both land and ocean. In addition, we can use the time series of measurements in horizontal and vertical extent and horizontal homogeneity to evaluate model predictions of long-range transport and vertical distribution of African dust. Analyses of PRiDE measurements will lead us to a better understanding of dust's optical, microphysical, and chemical properties, especially the significant parameters of dust single-scattering albedo and nonsphericity.

SAFARI-2000, August-September 2000, in the vicinity of South Africa

SAFARI focused on biomass burning in the savannah region of southern Africa. A multi-national effort, SAFARI is a critical part of the EOS Terra (MODIS, MOPITT, MISR, CERES and ASTER) science and validation mission. While in the region, we also studied Namibian marine stratus clouds at the end of SAFARI-2000.

This experiment involved the NASA ER-2 aircraft as well as the University of Washington CV-580 and two aircraft from the South African Weather Bureau. Primary instruments of interest for the ER-2 are the MAS, MOPITT-A, AirMISR, SSFR, LAS, S-HIS (simulating Terra instruments), and CPL (a lidar for profiling the atmosphere). The ER-2 coordinated with *in situ* aerosol, radiation, and chemistry measurements on the CV-580 and overflew numerous AERONET locations in Namibia, Botswana, South Africa, Zambia, and Zimbabwe. The ER-2 also overflew the SAVE/SMART site in Skukuza, South Africa. SAFARI marked one of the most aggressive and successful coupled ground-based, *in situ*, and remote-sensing campaigns ever in Africa. The research focuses on land-atmosphere processes. We aim to discover how emissions from fires, biomass, and human activity affect the biogeophysical and biogeochemical systems of southern Africa.

The SAFARI data revealed information about (1) the vegetation structure and underlying geology associated with it, (2) the evolution of thick haze and ozone, and the intricate structures within them, and (3) the interactions of haze—whether caused by industrial, biomass burning, marine or biogenic sources—with local and distant cloud fields. We also observed what appears to have been an unprecedented southern African fire season, especially in western Zambia, southern Angola, northern Namibia, and northern Botswana. Extremely large fires were common, lasting weeks, with fire fronts often exceeding 30 km, and with total burned areas covering hundreds of square miles. We have managed to characterize the land surface and the atmosphere before, during, and after such fires. Integrated airborne and ground-based activities coupled with remote sensing data acquisition from Landsat-7 and Terra enabled the thorough observation of four prescribed fires—two in Zambia and two in South Africa. Thus, the Terra team will benefit from comparing SAFARI observations with its retrieved surface reflectance, fire, burned area, vegetation, LAI/FPAR, water vapor, cloud, and aerosol products.

ACE-Asia, March-May 2001, in the vicinity of Northeast Asia

The International Global Atmospheric Chemistry program has organized a series of aerosol characterization experiments (ACE) to acquire data sets needed for assessing aerosol effects in major regions of the globe. ACE-Asia is designed to study the compelling variability in spatial and temporal scales of both pollution-derived and naturally occurring aerosols. These aerosols often exist in high concentrations over eastern Asia and along the rim of the western Pacific. Phase-I of ACE-Asia will take place from March to May 2001, in the vicinity of the Gobi desert, the east coast of China, the Yellow Sea, and Japan, along the pathway of Kosa (severe events that blanket east Asia with yellow desert dust, peaking in the spring season).

Central Asia is one of the most important dust sources. However, the climatic impact of central Asian dust is less well studied than that of Saharan dust. Asian dust typically originates in desert areas far from polluted urban regions. During transport, dust layers can interact with man-made sulfate and soot aerosols from heavily polluted urban areas. Added to the complex effects of clouds and natural marine aerosols, dust particles reaching the marine environment can have properties drastically different from dust particles at the source. Thus, information about the unique temporal and spatial variations of Asian dust is of special importance in understanding regional-to-global climate issues such as radiative forcing, the hydrological cycle, and primary biological productivity in the mid-Pacific Ocean.

In collaboration with international chemists, our main goal in ACE-Asia is to use SMART instruments to continuously measure aerosol optical/radiative properties, column precipitable water, and surface reflectivity over homogeneous areas. Including flux measurements in our scope permits us to determine dust aerosol radiative flux, in addition to measuring loading and optical thickness. At the time of the MODIS overpass, these ground-based observations can provide valuable data to compare with MODIS retrievals over land. Even without dust events, the homogeneity of the Gobi desert serves as an excellent calibration target. Thus, SMART observations in the vicinity of dust sources are our first priority. A less instrumented SMART version will be set up in the marine environment.

Si-Chee Tsay, Code 913 (Si-Chee.Tsay.1@gsfc.nasa.gov)

SAVE/SAFARI-2000 Ozonesonde Launches in Lusaka, Zambia

As part of the SAVE component of SAFARI 2000, Laboratory staff launched balloon-borne ozonesondes in Zambia, Lusaka. The ozonesondes measured ozone, temperature, pressure, and relative humidity during the SAFARI-2000 dry season activity. Our objective was to validate tropospheric ozone data derived from the TOMS-EP satellite. The ozonesonde lab set-up was at the Zambian Meteorological Department (ZMD), where it was easy to put the ozonesonde-telemetry antenna on the adjacent roof and coordinate activity with the ZMD's radiosonde launches (taken twice daily at 1230 and 0030 local time).

The data gathered were outstanding because the burning of the late dry season took off at an explosive rate in late August and early September. These were the first ozone soundings taken in the heart of the central southern African burning region. The combination of stagnant conditions with intense local sources of ozone precursors produced peaks of > 100 ppbv ozone below 6 km and surface ozone > 70 ppbv at the end of a day. On the first sounding day there was a trash fire 50 meters from the ozonesonde launch site at ZMD (see Figure 9). Daily microTOPS (hand-held sun photometer) measurements of aerosol optical thickness were 1.5-2.0 in the visible-near UV. These aerosol and ozone values are higher than values seen at regular SHADOZ ozonesonde launching stations (e.g. Irene, South Africa, and Nairobi, Kenya) and SAFARI-1992 sites that are often hundreds of kilometers downwind from the densest fire activity.

Figure 10 shows tropospheric ozone derived from TOMS-EP for the September 8 launch. The triangle marks the location of the launch site in Lusaka (15.4S, 28.3E). The ozonesonde profile for the tropospheric portion of the flight (right panel) is in excellent agreement with the satellite-derived tropospheric ozone. Representing the burning season in southern Africa, Figure 10 suggests that the heaviest burning occurred in western and eastern central Africa. TOMS also measures high smoke aerosol over these regions. Exit pathways for these pollutants are east to Madagascar and the Indian Ocean, and west over the Angolan escarpment. As the ozone and smoke head toward the Atlantic Ocean, they are lifted over the mountains and are concentrated over the eastern Atlantic in a region of sinking and recirculating air motions. The TOMS-EP satellite followed smoke and tropospheric ozone ("smog ozone") day-by-day from biomass fires as they were transported long distances from burning areas. Animations of ozone and smoke transport over southern Africa can be seen at http://www.gsfc.nasa.gov/gsfc/earth/environ/safari2000_1final.htm

The SAFARI-2000, Lusaka ground-truth effort discovered that, besides the well-known large fires over central African grasslands, urban fires produced serious pollution because of preparation of charcoal for burning trash, cooking, and heating. The haze layer (containing high levels of ozone - a component of smog) was heavier than we expected from these fires observed by ground-based researchers, the Terra and Landsat 7 spacecraft, and research aircraft.

The NASA projects served by this trip were (1) SHADOZ (Southern Hemisphere ADditional OZonesondes - http://code916.gsfc.nasa.gov/Data_services/shadoz/), and (2) SAVE, as part of (3) SAFARI-2000 (http://safari.gecp.virginia.edu/).

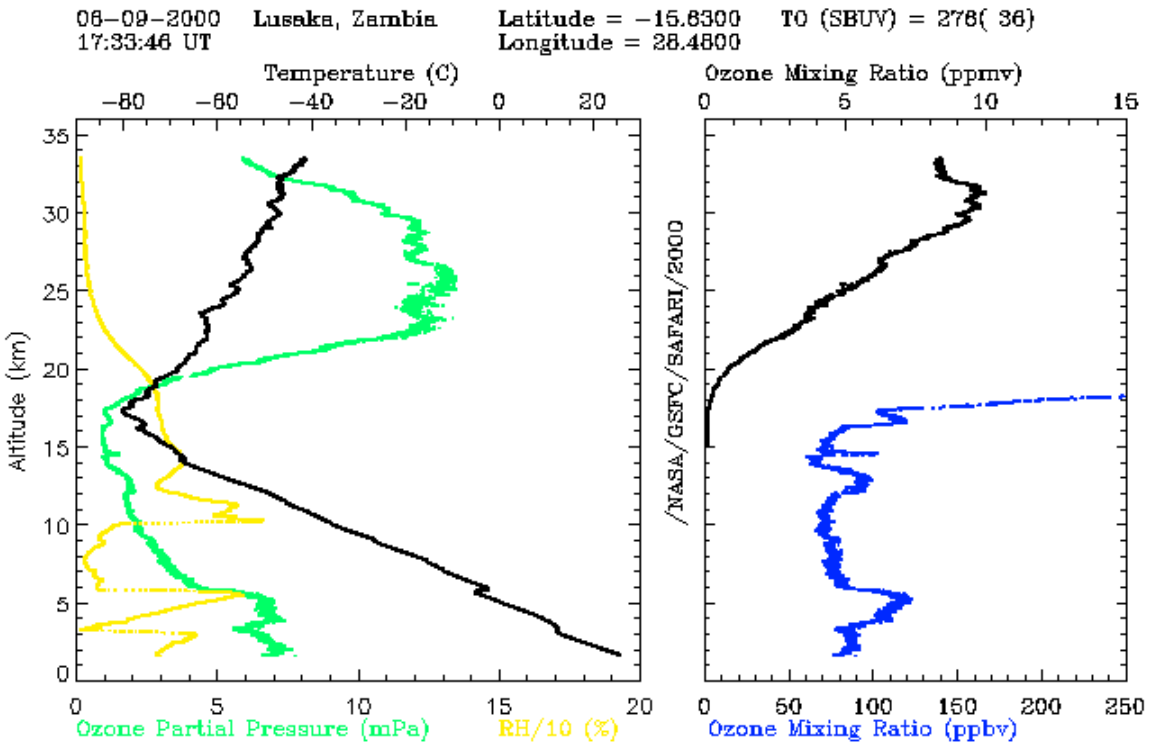

Figure 9. Ozone, water vapor, and temperature soundings taken in the heart of the central southern African burning region during SAFARI.

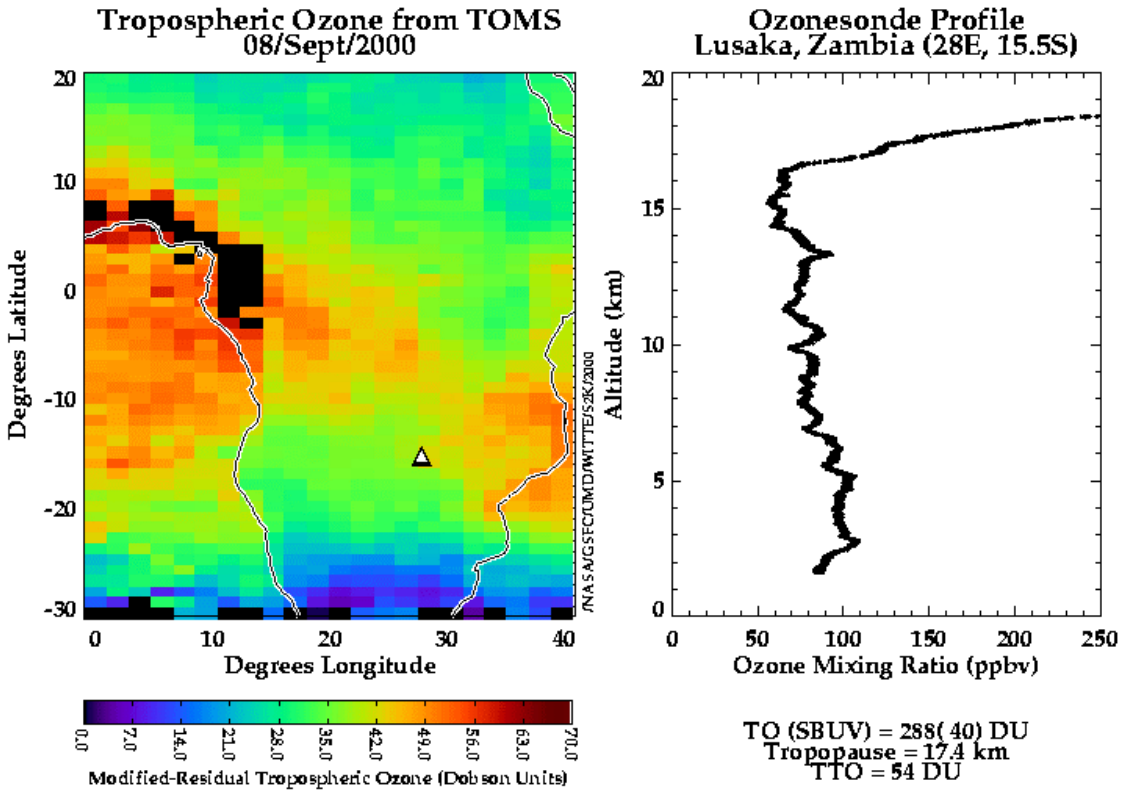

Figure 10. Tropospheric ozone derived from TOMS-EP for the September 8 launch during SAFARI.

Anne M. Thompson, Code 916 (Anne.M.Thompson.1@gsfc.nasa.gov)

Airborne ER-2 Cloud Physics Lidar System

During 2000, a new airborne lidar system was added to the Laboratory's instrumentation capabilities. The Cloud Physics Lidar (CPL) is specifically designed for use on the ER-2 aircraft and provides the first high-altitude photon-counting lidar capability. The CPL will enhance cloud and radiation studies by providing high-resolution profiles of clouds, aerosols, and smoke layers.

The CPL is a state-of-art system. It employs a solid-state, diode-pumped, conductively cooled laser operating at 5 kHz repetition rate. The laser simultaneously transmits 1064 nm, 532 nm, and 355 nm radiation. The receiver uses solid-state photon-counting detectors to measure the backscattered light at all three wavelengths. In addition, the 1064 nm signal is used for a depolarization measurement. Measuring the backscattered signal at three wavelengths provides information about cloud and aerosol optical properties. The depolarization measurement can be used to determine the molecular phase of clouds.

After construction, the CPL was immediately deployed on the SAFARI-2000 field campaign during August and September 2000. The purpose of SAFARI-2000 was to study aerosol and smoke layers over the southern African continent. During the SAFARI-2000 campaign, 19 science missions were flown, producing nearly 100 hours of data. The CPL functioned properly on all flights and the resulting data show remarkable detail of the boundary layer aerosol and smoke layers that prevailed over the African continent. Figure 11 displays a typical example of the CPL data, showing the intense boundary layer aerosol and stratified smoke/aerosol being lifted high into the atmosphere, as well as intermittent clouds.

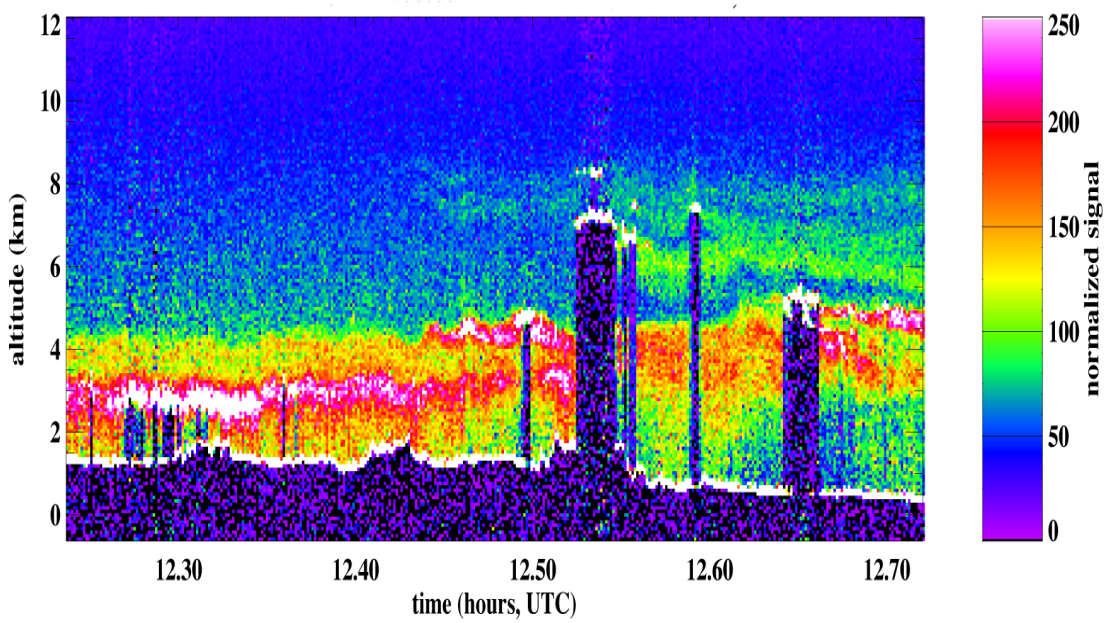

Figure 11. Example of 532 nm CPL data from SAFARI-2000 campaign, September 17, 2000. Data shows a complicated atmosphere including boundary layer aerosol and smoke, intermittent clouds, and smoke/aerosol being advected in at high altitudes. Data shown is normalized photon counts. Altitude is above sea level, and the bottom white line is the terrain profile. Cloud shadows are present whenever the lidar signal cannot penetrate through a layer.

Matt McGill, Code 912 (Matthew.J.McGill.1@gsfc.nasa.gov)

Instrument Development

Geoscience Laser Altimeter System (GLAS)

Global spaceborne lidar profiling of the true height structure of clouds and aerosol in the atmosphere is within a year of reality. The EOS Geoscience Laser Altimeter System (GLAS) instrument is being completed at GSFC. The clouds and aerosol lidar research group has contributed to major parts of the instrument development and the development of science algorithms. Stan Scott is responsible for the assembly and testing of the 532-nm lidar receiver system. The lidar receiver system is to be completed in 2000.

We have completed the initial version of the data processing algorithms for the GLAS atmospheric science data products. These highly complex algorithms must be able to take data and produce measurement results in real time.

The GLAS instrument will measure the vertical structure of radiatively significant clouds and aerosols with sufficient vertical and horizontal resolution to resolve large-scale variability. The atmospheric structure will be measured full-time over the entire orbital cycle including sunlit and dark scenes. The processing and retrieval algorithms will produce seven core data products. These are: (1) atmospheric layer type and vertical location, (2) aerosol backscatter cross section profile, (3) cloud backscatter cross section profile, (4) aerosol extinction cross section profile, (5) cloud extinction cross section profile, (6) aerosol optical depth per layer, and (7) cloud optical depth per layer. Layer locations are a direct measurement result from lidar-scattering structure. The basic parameter that defines the integrated radiative influence of a layer is optical depth. The GLAS instrument will be able to sense layers up to an approximate total optical depth of two before the signal is extinguished. The vertically resolved structure of radiative forcing is directly related to the extinction cross section profile. Both the extinction cross section and optical depth are derived parameters that involve the height-resolved laser backscatter data and appropriate retrieval algorithms. A simulation of the GLAS 532 nm signal for nighttime and daytime conditions is given in Figure 12, using TOGA-COARE data.

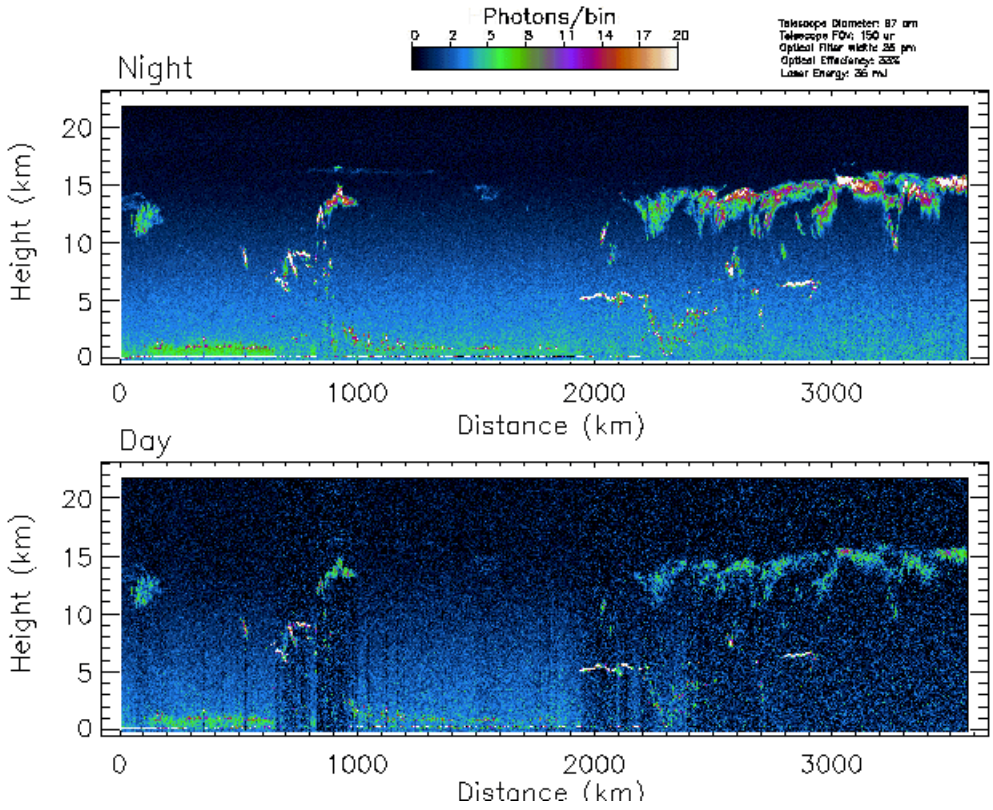

Figure 12. A nighttime (upper panel) and daytime (lower panel) simulation of the GLAS 532 nm signal using data from the TOGA-COARE experiment. The color coding is in terms of photons per bin (75 meters) as indicated on the color bar at the top.

James Spinhirne, Code 912 (James.D.Spinhirne.1@gsfc.nasa.gov)

GSFC Airborne Raman Ozone, Temperature, and Aerosol Lidar (AROTEL)

The GSFC Airborne Raman Ozone, Temperature, and Aerosol Lidar (AROTEL) is a new instrument that was developed for operation on board the NASA DC-8. AROTEL flew on its first mission during the SAGE III Ozone Loss Validation Experiment (SOLVE) in the winter of 1999 – 2000. The aircraft was deployed to Kiruna, Sweden, on three separate occasions throughout the winter, with approximately 7 flights into the Arctic vortex on each deployment.

The instrument is a collaborative effort between scientists at Goddard and Langley, a collaboration which has worked well and has resulted in a better system, scientifically, than would have been achieved if either group had proceeded on its own. The instrument is ideally suited for studies of ozone and clouds. The measured temperature provides important meteorological data, and the aerosol parameters measured at three widely spaced wavelengths constrain the calculations of microphysical properties within clouds (PSCs or tropical cirrus). The instrument generates a self-consistent set of data, in that the temperature and relative density profiles returned from the 355/387 data are used in the retrievals for aerosols and ozone mixing ratio. We are therefore not dependent on assimilations, which are based on data that could be twelve hours or more away from the lidar data**.**

Figure 13 shows data from the IR/Vis aerosol channels for the flight of Dec. 10, 1999. A thin NAT polar stratospheric cloud is seen at approximately 19-21 km at 13:50. NAT is typically thought of as forming near 195 K, but from Figure 14, we can see a large volume of the stratosphere with temperatures at 192 K with no PSCs evident. This data has spurred more research into the physics of PSC formation.

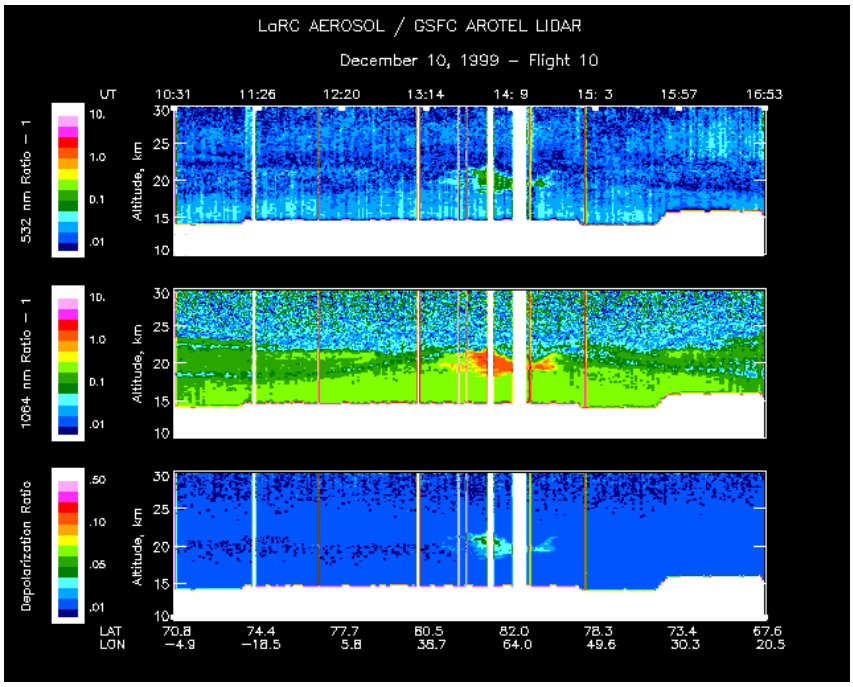

Figure 13. Aerosol scattering ratio data from 12/10/99. A thin liquid NAT cloud can be seen at ~13:50. Fine structure in the background aerosol is also seen.

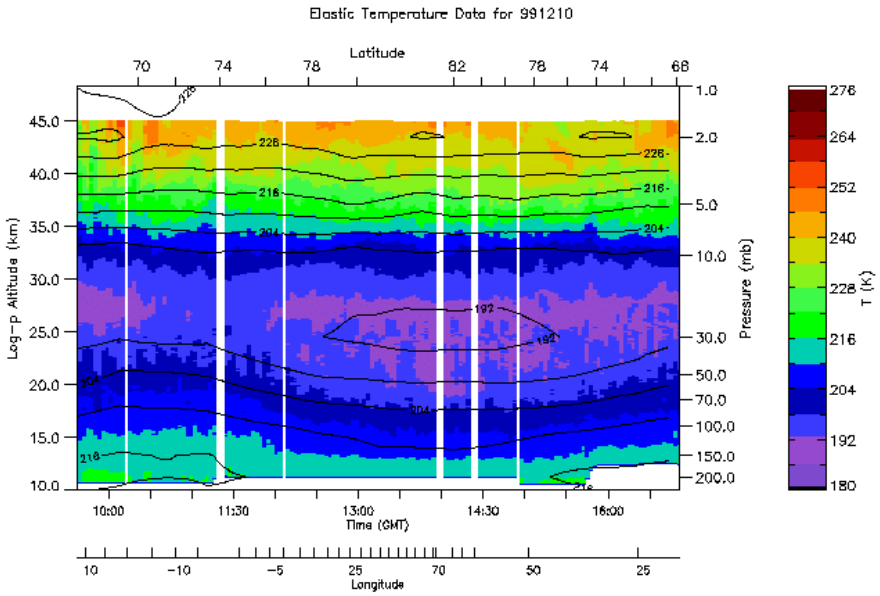

Figure 14. AROTEL temperatures above the aircraft.

The use of Raman scattering for the retrieval of temperatures in the presence of optically thin polar stratospheric clouds is a first for the DC-8. Figures 15 and 16 show the improvement achieved by using this technique as compared to using purely elastic scattering. Since Raman scattering depends only on the gas that provides the wavelength shift, there is no signature from aerosol scattering in these returns, only a slight effect due to extinction. When clouds are optically thin, the Raman return is representative of the atmospheric number density, and we can retrieve a reliable temperature.

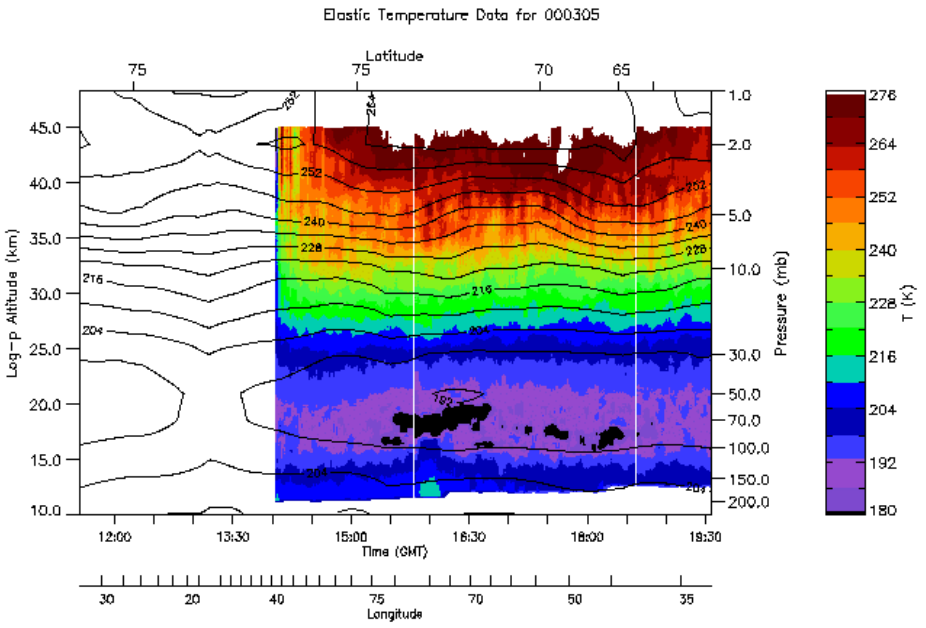

Figure 15. Temperature retrieved on March 5, 2000 using elastically scattered returns. Note the black, anomalously cold areas where PSCs are present.

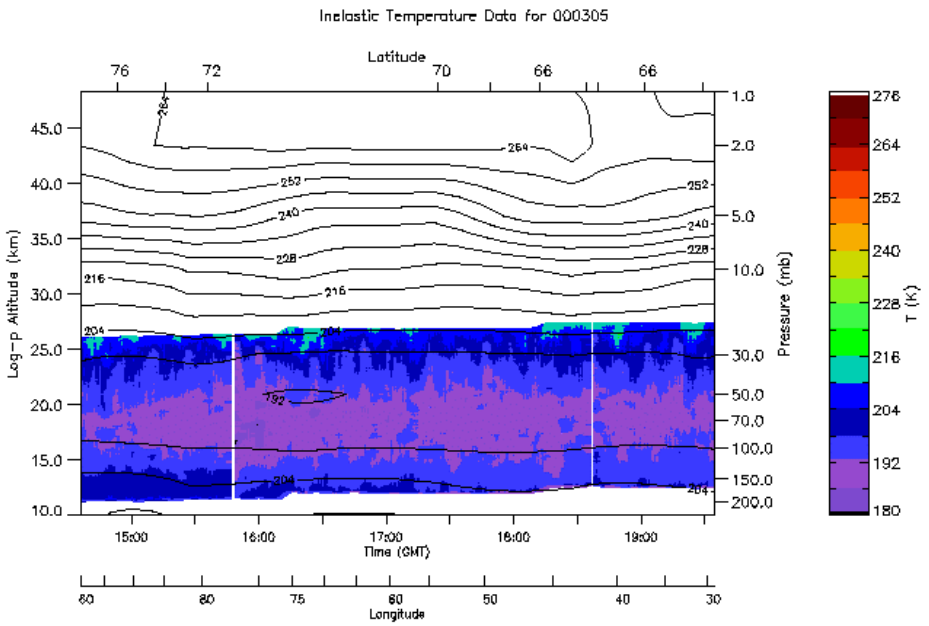

Figure 16. March 5, 2000 temperature retrieved from Raman scattered returns. The black anomalously cold regions have been removed.

Ozone as a function of altitude is also retrieved from the lidar returns, using a differential absorption (DIAL) technique. The 308 radiation is absorbed by ozone and the 355 radiation is used as the atmospheric reference. Figure 17 shows ozone measured above the aircraft along the flight track from Dryden Research Center to Kiruna, Sweden, on February 27, 2000. The transit across the vortex edge can be seen at approximately 74N. Data from these types of measurements within the Arctic vortex were used to calculate the ozone loss rate between mid-January and mid-March. This loss rate, shown in Figure 18, with a maximum loss at about 460 K, amounted to absolute losses in ozone up to 65% at this altitude. In the Antarctic, total ozone loss at some altitudes is observed. From the AROTEL measurements during the SOLVE campaign, we observed that this was a very cold winter and that PSCs, which process the air and initiate the chemistry that leads to the springtime ozone loss, were ubiquitous throughout the Arctic vortex.

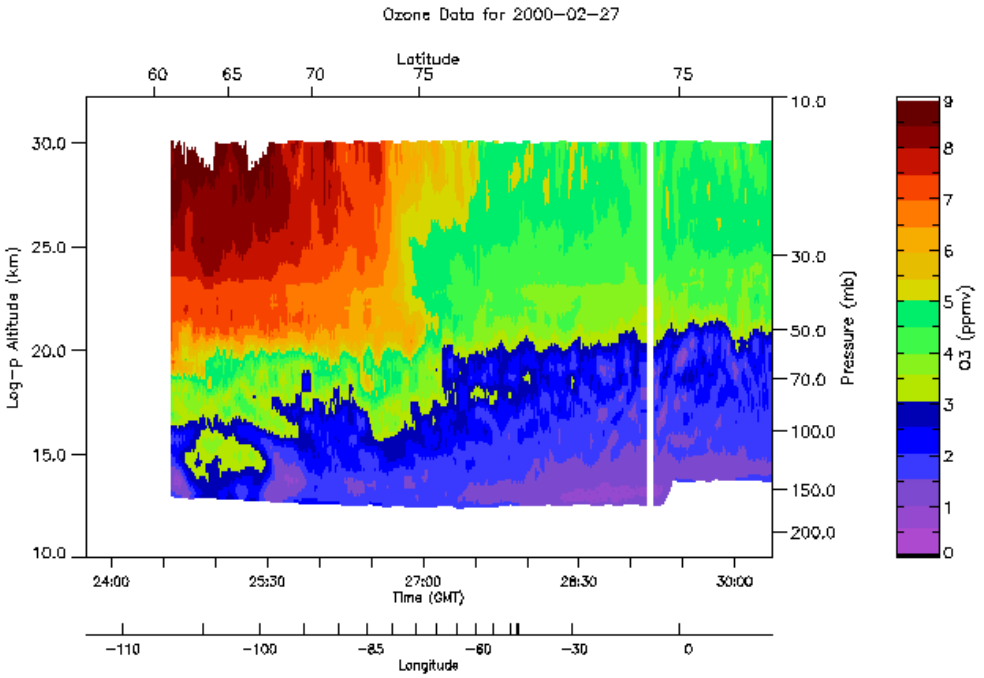

Figure 17. Ozone above the aircraft during the transit flight of January 27, 2000. The vortex edge is very well-defined.

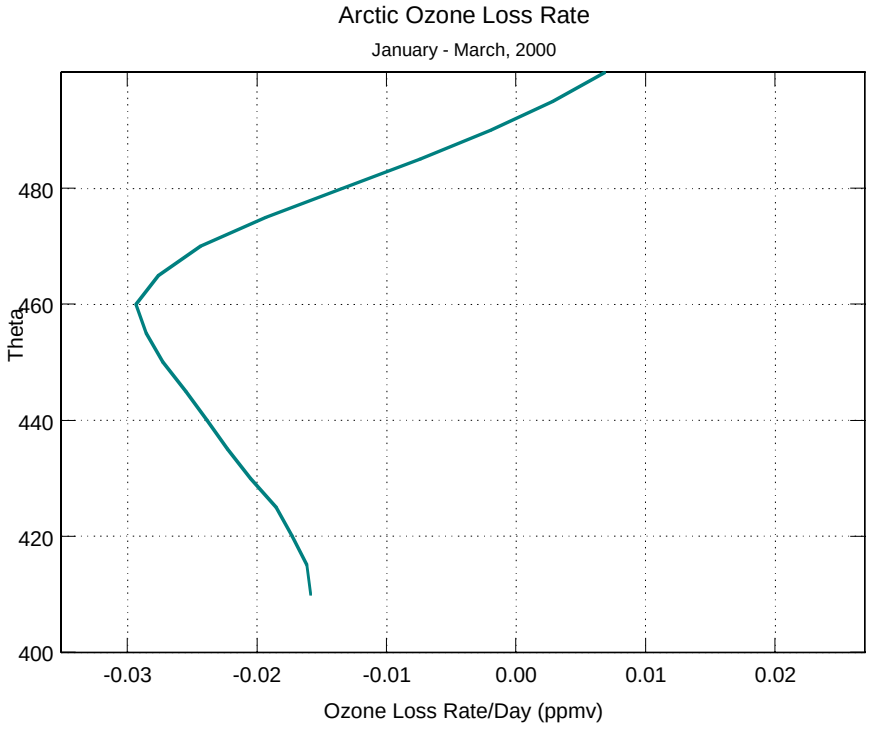

Figure 18. Plot of the ozone loss rate from mid-January to mid-March, 2000, as a function of potential temperature.

Thomas J. McGee, Code 916 (Thomas.J.McGee.1@gsfc.nasa.gov)

Data Analysis

Aerosol Studies

Operational Use of MODIS/Terra Data for Monitoring Fires in Montana and Idaho

We used images from MODIS and MOPITT to gather information on wildfires in Montana and Idaho. In fact, during the fires of August 2000, we were able to deliver images to the U.S. Forest Service within 24 hours of real time.

Little snow fell across North America in the winter of 1999-2000. Figure 19, a MODIS 8-day composite from March 512, shows much less snow cover than the 30-year averages for February (yellow line) and March (red line). The lack of snow contributed to near-record low water levels in the Great Lakes. Low water levels and dry soil made conditions ripe for an active wildfire season in the west and mid-west. The literature suggests that signature outgoing longwave radiation (OLR) anomalies precede drought events in North America by about 10 days. The CERES instrument aboard TRMM measured low OLR values off the west coast and high values over the Gulf of Mexico and southeastern U.S. (not shown).

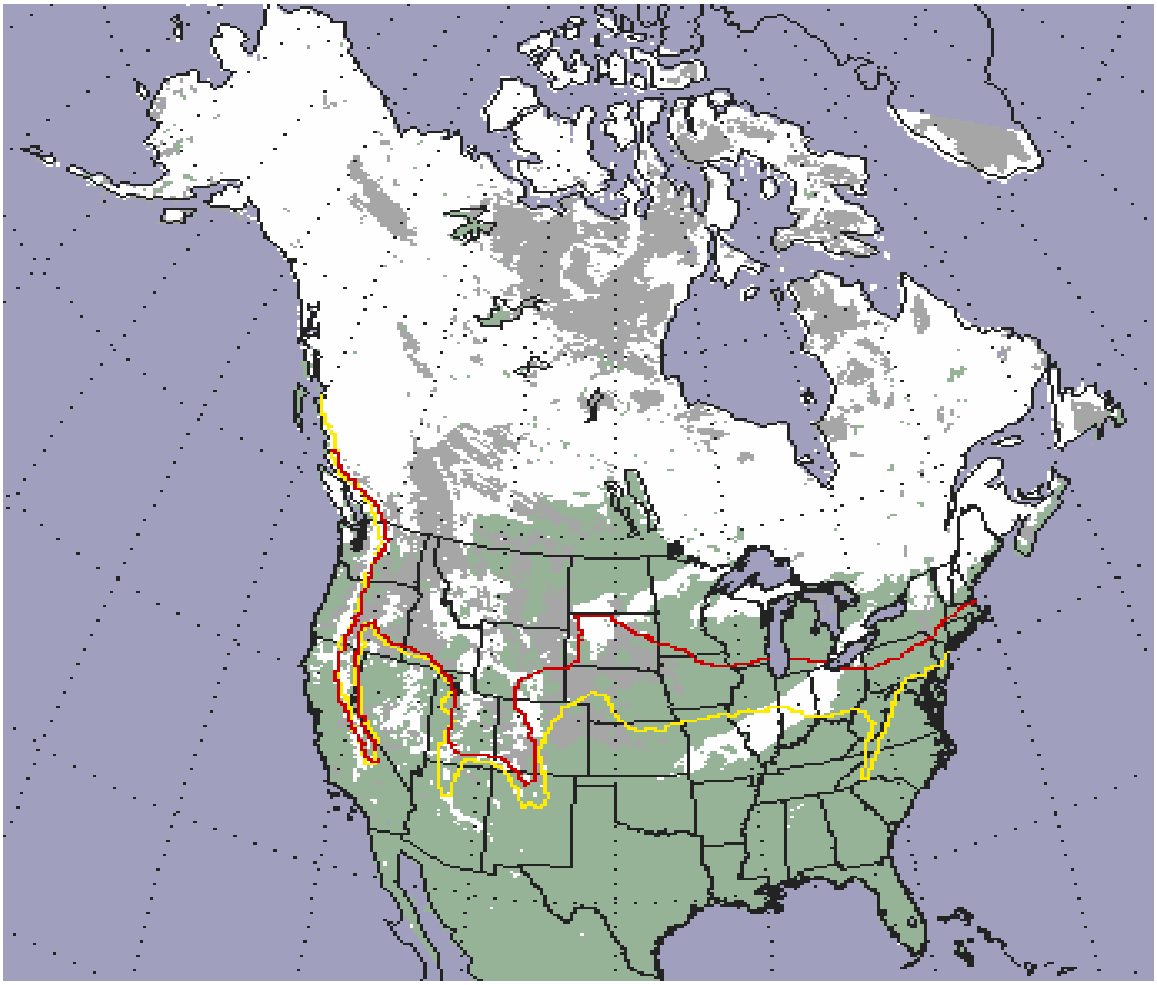

Figure 19, MODIS 8-day composite from March 512, showing much less snow cover than the 30-year averages for February (yellow line) and March (red line).

As has happened in the wake of 16 of the last 19 La Niña events, a large anti-cyclone formed over the central United States, effectively blocking the usual flow of water vapor from the Gulf of Mexico into the region. MODIS data acquired on April 17, 2000, confirms this effect (not shown). Drought conditions worsened and the region became increasingly susceptible to wildfires.

Disaster struck the Bitterroot Valley region of Montana in early August. A wildfire ignited and spread rapidly, spilling over into Idaho and consuming millions of acres over the next 5 weeks. The true-color image below was acquired on August 5 by MISR (Figure 20). On August 29, President Clinton declared parts of Montana and Idaho as disaster areas due to the extensive fire damage.

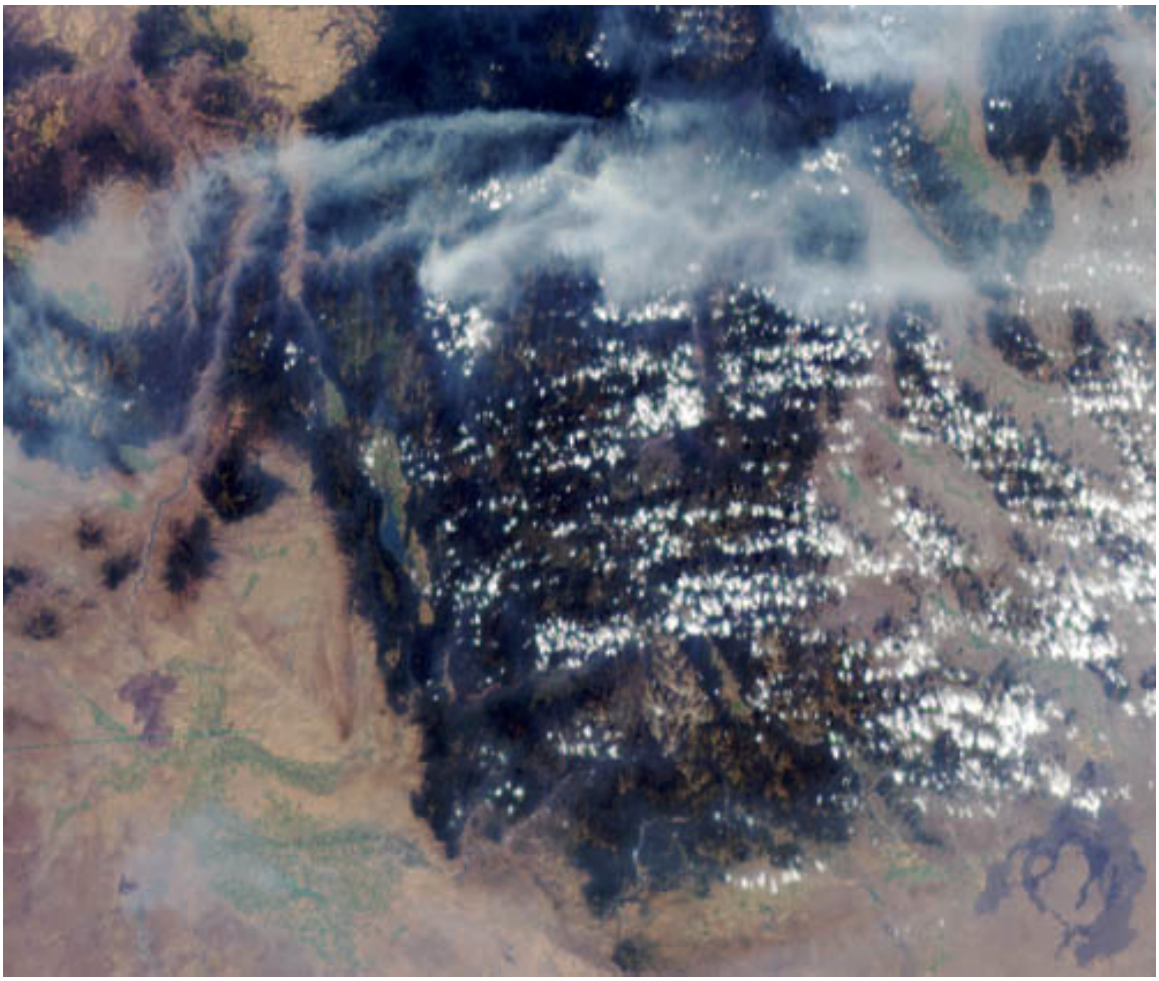

Figure 20. True color image of Idaho acquired on August 5 by MISR on the Terra spacecraft showing smoke from the wild fires.

On the same day, Terra Project Scientist Yoram Kaufman asked the MODIS and Terra Rapid Response teams to begin providing MODIS data operationally to the U.S. Forest Service to aid in the Service's efforts to contain and extinguish the fires. On August 30, the MODIS Team produced a true-color image over Montana and Idaho (Figure 21) that showed the smoke and burn scars, along with the locations of actively burning portions of the wildfires, as observed by MODIS on August 23. At that time, it took the Rapid Response team a week or more to turn around MODIS images.

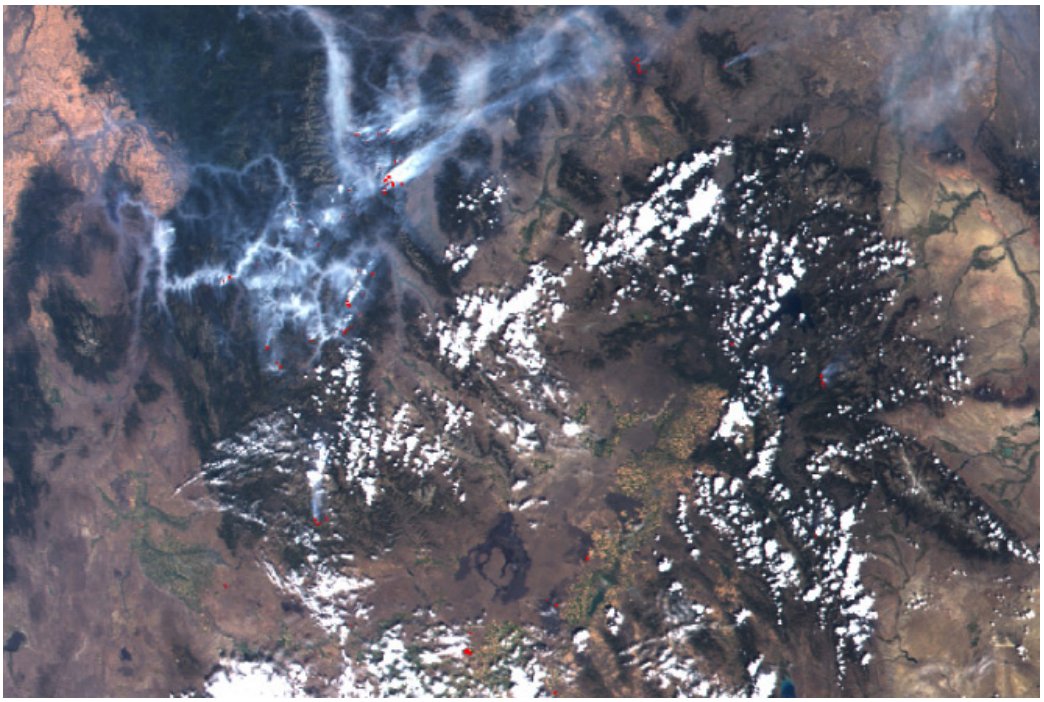

Figure 21. Terra MODIS true-color image of fires over Montana and Idaho on August 23 showing the smoke and burn scars, along with the locations of actively burning portions of the wildfires, image produced on August 30. The red dots are saturated pixels where burning is taking place.

The goal in this exercise was to achieve 24-hour turnaround. On August 31, we succeeded in turning around these MODIS images of Idaho acquired on August 30 (Figure 22).

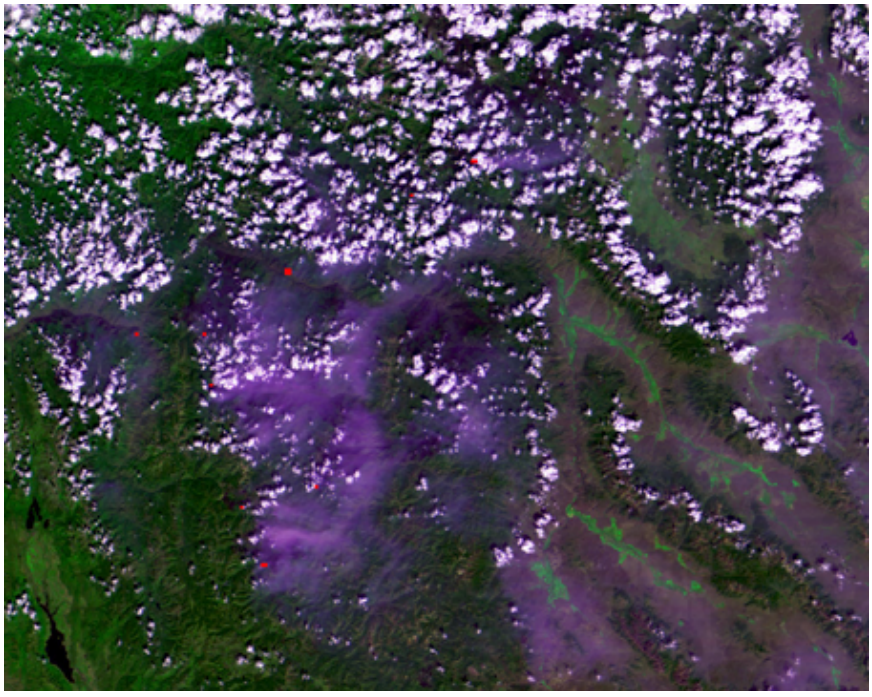

Figure 22. MODIS color composite image of fires in Idaho taken August 30, and processed on August 31 by the Terra Rapid Response team aiding the U.S. Forest Service.

The Terra satellite has also demonstrated some of its potential for new, synergistic approaches to studying Earth events using multiple sensors. For instance, this MOPITT image (Figure 23) shows the levels of carbon monoxide generated by the fires during the period during August 22-27.

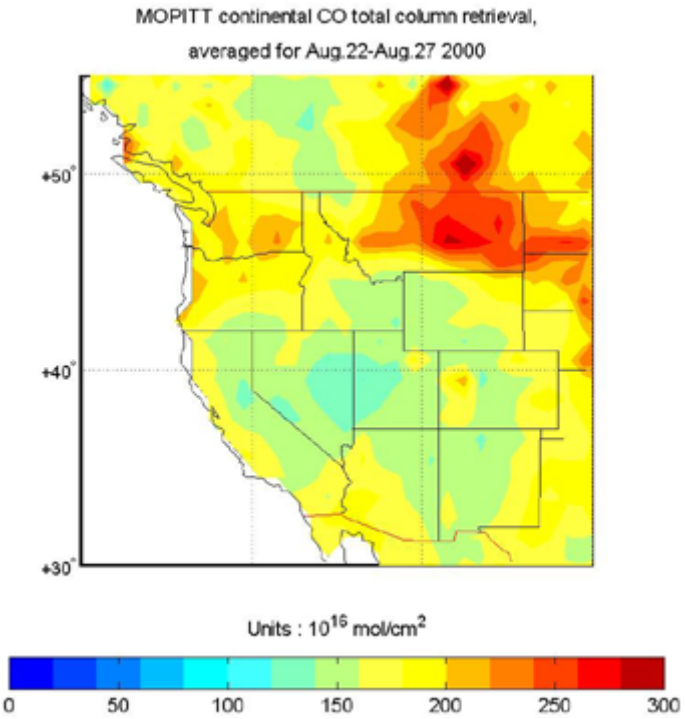

Figure 23. MOPITT image showing the levels of carbon monoxide generated by the fires during August 22-27.

The MODIS images, below, demonstrate MODIS' superior sensitivity to fire intensity as compared to AVHRR (Figure 24). Because MODIS fire channels have a higher saturation threshold, they provide a better gauge of where the hottest parts of the fire are located. In these images, color is a proxy for temperature.

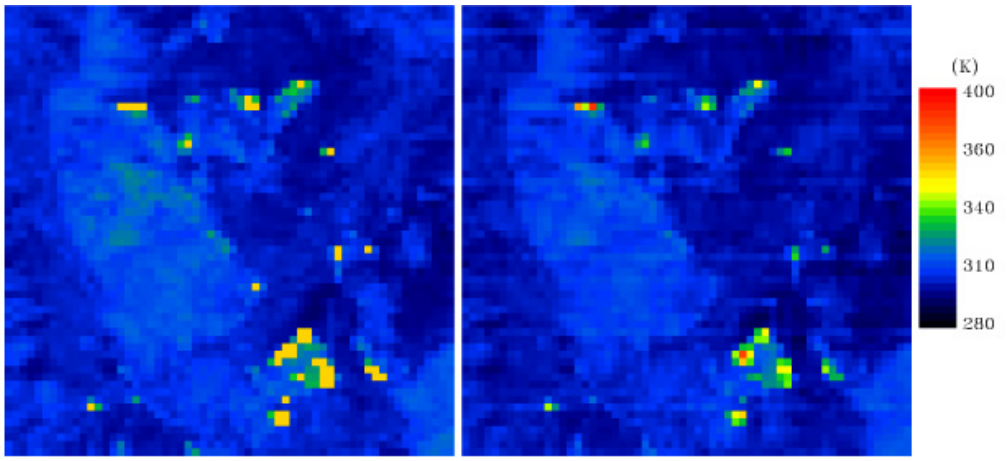

Figure 24. MODIS images in channels 20 and 21 showing sensitivity to fire intensity.

This image (Figure 25) shows the Clear Creek fire in Idaho on the morning of August 30, 2000, as seen by the Advanced Spaceborne Thermal Emission and Reflection Radiometer (ASTER). The image combines a color composite of near-infrared, red, and green light at 15-meter (49-foot) resolution with thermal infrared data at 90-meter (295-foot) resolution.

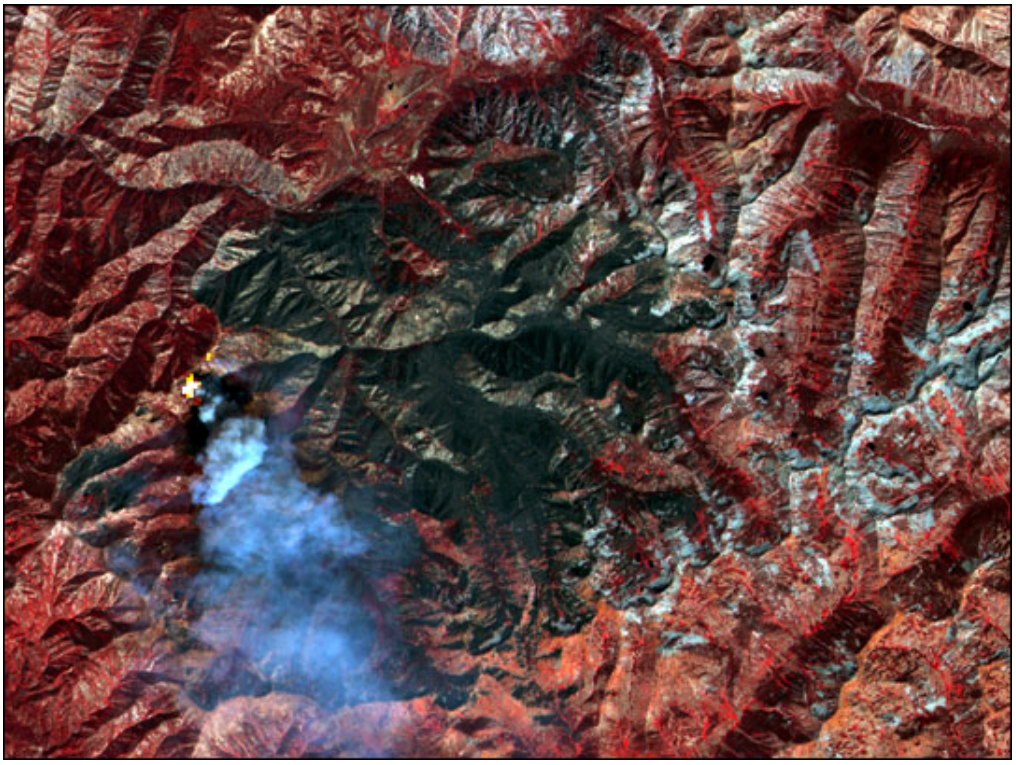

Figure 25. ASTER image of the Clear Creek fire in Idaho on August 30 combining near infrared, red, and green light at 15 m resolution with thermal infrared at 90 m resolution.

Yoram Kaufman and David Herring, Code 913 (Yoram.J.Kaufman.1@gsfc.nasa.gov, David.D.Herring.1@gsfc.nasa.gov)

Smoke Aerosol from Biomass Burning in Mexico, Hygroscopic Smoke Optical Model

We used data from Mexico, South America, and Africa to characterize regional variations in smoke generated by biomass burning.

In 1998, an especially dry spring created an intense fire situation in the tropical areas of southern Mexico and Central America. Fires burned out of control for weeks and covered the region with thick smoke. In May, wind carried the smoke northward into the United States, where it was observed as far north as Wisconsin. The event generated much attention within the United States, but was otherwise typical. In the tropics, biomass burning occurs globally and produces vast quantities of smoke that can cover regions as large as half a continent.

The smoke particles, called smoke aerosol, play a role in the Earth's energy balance by directly reflecting solar radiation back to space and by altering cloud properties that indirectly change cloud reflectance and rain production efficiency. We still do not understand exactly how the smoke aerosol affects the energy balance and changes climate. Much of our ignorance arises from a lack of understanding of the physical and optical properties of the particles themselves. Do

these properties vary by geographic region? If so, is there a physical model that can describe the variation?

We analyzed the data acquired from the 1998 Mexico event in conjunction with chemical data collected in the United States and Sun/sky radiometer data collected in North and South America and Africa. The combination of these data sets results in a simple physical model that explains the regional variation in smoke properties as a function of particle water vapor absorption and variability in light absorbing carbon content.

Data from the Interagency Monitoring of Protected Visual Environments (IMPROVE), a network of aerosol measuring systems distributed across the United States, provides the chemical composition of the aerosol. We use the IMPROVE observations at Big Bend National Park (BBNP), located along the Mexican border in south Texas, to identify biomass burning aerosol with a chemical indicator. The identified smoke aerosol shows a higher sulfate component at BBNP than at other stations measuring biomass burning aerosol in the United States and in South America. The larger fraction of sulfate, a byproduct of industry, is not surprising, as the smoke plume from the tropical regions passed over sources from major industrial regions and power plants in central and northern Mexico. Sulfates are strongly hygroscopic substances meaning that they readily absorb water from their environment. A larger fraction of sulfate in an aerosol particle suggests that these particles will be more strongly hygroscopic than similar particles with less sulfate.

Because the Mexican smoke particles have a larger hygroscopic component than smoke from other regions, we expect these particles to absorb more water and thus be larger, with a larger single-scattering albedo (ω_o). Single-scattering albedo is the ratio between a particle's scattering and extinction coefficients. Larger ω_o, therefore, indicates more scattering and less absorption. A particle grows in size as it takes in water and simultaneously dilutes the light absorption materials of the particle. The AErosol RObotic NETwork (AERONET), a global network of Sun/sky radiometers, provides size and optical properties of smoke from Mexico, South America, and Africa. AERONET data show that, indeed, Mexican smoke consists of larger particles exhibiting less light absorption (larger ω_o) than similar particles from other tropical biomass burning regions. We have established a consistent physical model that shows that water up-take alone can explain the geographical variation in the particle size (Figure 26a). However, water alone cannot account for the variation in light absorption (variation in ω_o). Variations in light absorbing carbon (LAC) are also necessary. As Figure 26b shows, the global variation in particle light absorption (single scattering albedo – ω_o) can be explained by a physical model that combines a hygroscopic model with the variations of LAC measured in different locations.

Our hygroscopic smoke aerosol model demonstrates that the particle size and optical properties are not independent, but vary in tandem with variations in the particle's readiness to absorb water and with variations in light absorbing carbon amounts. The results imply that these broad, interconnected variations in smoke aerosol properties are important to both the accurate assessment of the global effects of biomass burning aerosols on climate and the remote sensing of such aerosols from space.

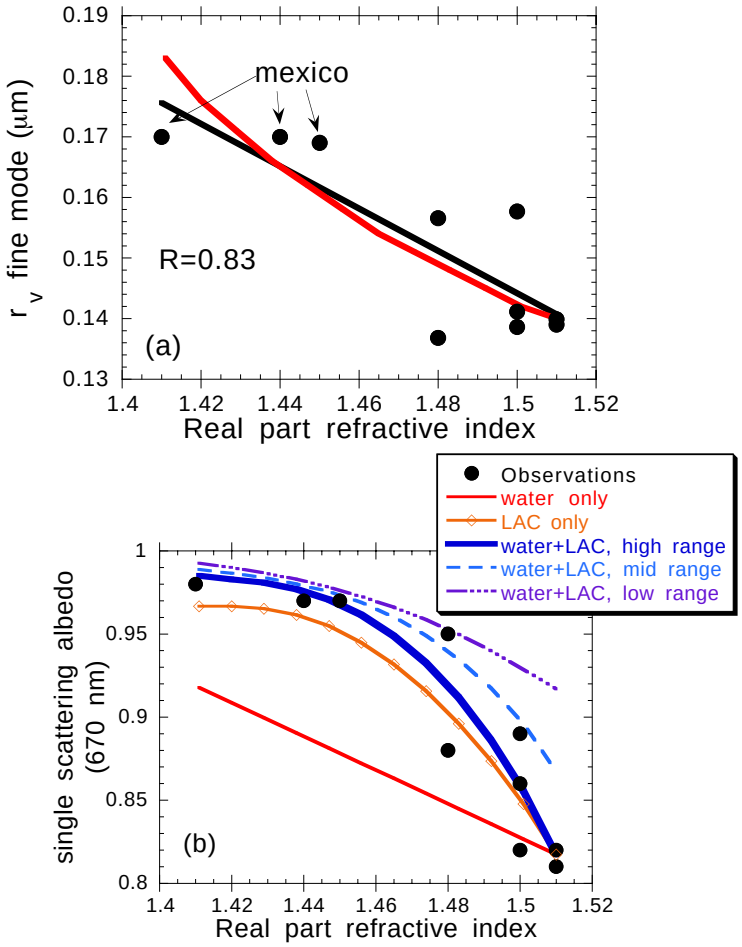

Figure 26. The figure shows smoke particle size (r_v), top (26a), and single-scattering albedo at 670 nm (ω_o), bottom (26b), as functions of the real part of the refractive index, n_r, for several stations in Mexico, Africa, and South America. The data represents mean conditions for optical thickness at 670 nm near 0.50. The points representing Mexican aerosols are identified in the top panel. In the top panel (26a) the black line is the best fit through the data points with the correlation coefficient given. The red line represents a particle size growth model dependent only on water uptake. In the bottom panel (26b) the red line represents the same water only model of the top panel. The orange line represents a dry model with varying light absorbing carbon (LAC). The other lines represent wet models with varying LAC as observed in smoke-affected aerosols from Africa, South America, and the Mexican event.

Lorraine A. Remer, Code 913 (Lorraine.A.Remer.1@gsfc.nasa.gov)

Clouds and Precipitation

Accuracy of TRMM Monthly Rainfall Maps

One of the primary data products of the Tropical Rainfall Measuring Mission (TRMM) satellite is monthly maps of rainfall. For instance, Figure 27 shows gridded TRMM estimates of the rainfall for the month of January 1998 on a 2.5° grid over the Pacific Ocean within 10° of the equator. In order to use such maps for such quantitative work as comparisons with seasonal forecast models or studies of the global water balance, we need some measure of the accuracy of the rainfall estimates in each grid box.

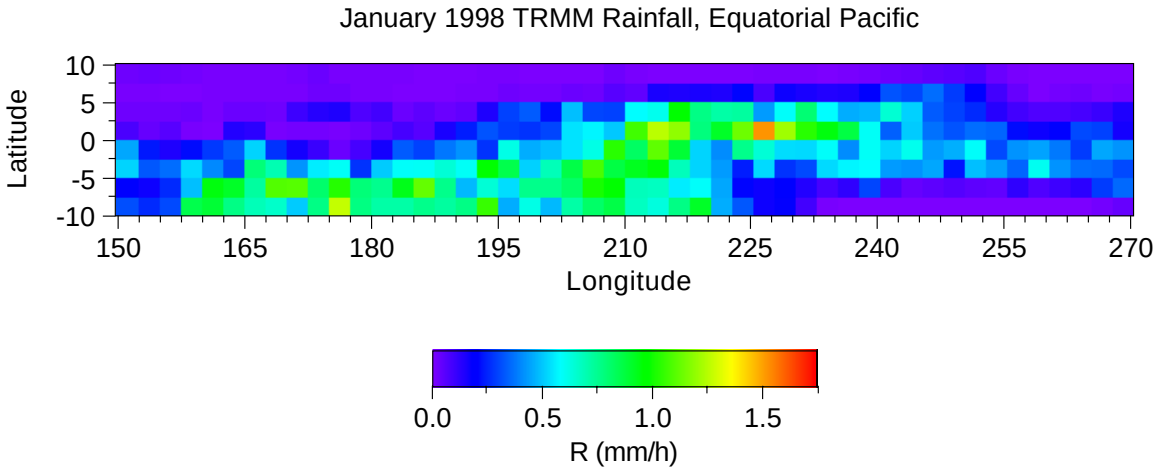

Figure 27. A gridded map of monthly rainfall typical of those produced from TRMM rain data. Enhanced amounts of rainfall can be seen in the central Pacific typical of the large El Niño episode in progress at that time.

The TRMM estimates of monthly rainfall in each grid box can be in error for two reasons: (1) Errors occur in trying to estimate rainfall with remote-sensing methods based on microwave radiation from the precipitating systems, and (2) the satellite cannot view the grid box continuously, since the satellite views grid boxes only about once per day on average. We have developed a method for estimating the root-mean-square (rms) "random" component of this error, denoted by σ_E.

The method predicts that the rms error of satellite averages should be proportional to the variability of area-averaged rain rate, which can be directly estimated from the satellite data. The method was tested using rainfall estimates obtained from two orbiting Defense Meteorological Satellite Program (DMSP) satellites carrying microwave instruments, the Special Sensor Microwave/Imagers (SSM/I), similar to those on TRMM. By comparing the two SSM/I estimates of rainfall for the same month and grid box, we can estimate the random error σ_E in monthly averages of rainfall from the satellites. Estimates of mean squared errors σ_E^2 are plotted versus a measure of the variability in grid-box averages of rain rate, σ_A^2, in Figure 28. They are indeed proportional, as predicted. We can estimate the proportionality constant by knowing the frequency of visits by the satellite and the time correlation of area-averaged rainfall. The proportionality constant is not sensitively dependent on the time correlations of rainfall. Thus, we can make reasonably accurate estimates of the proportionality constant from satellite data alone. It is therefore possible to provide estimates of the amount of random error present for each grid-box average in maps like that in Figure 27. The method is described in a paper to appear in the *J. Appl. Meteor.* (Bell et al. 2001).

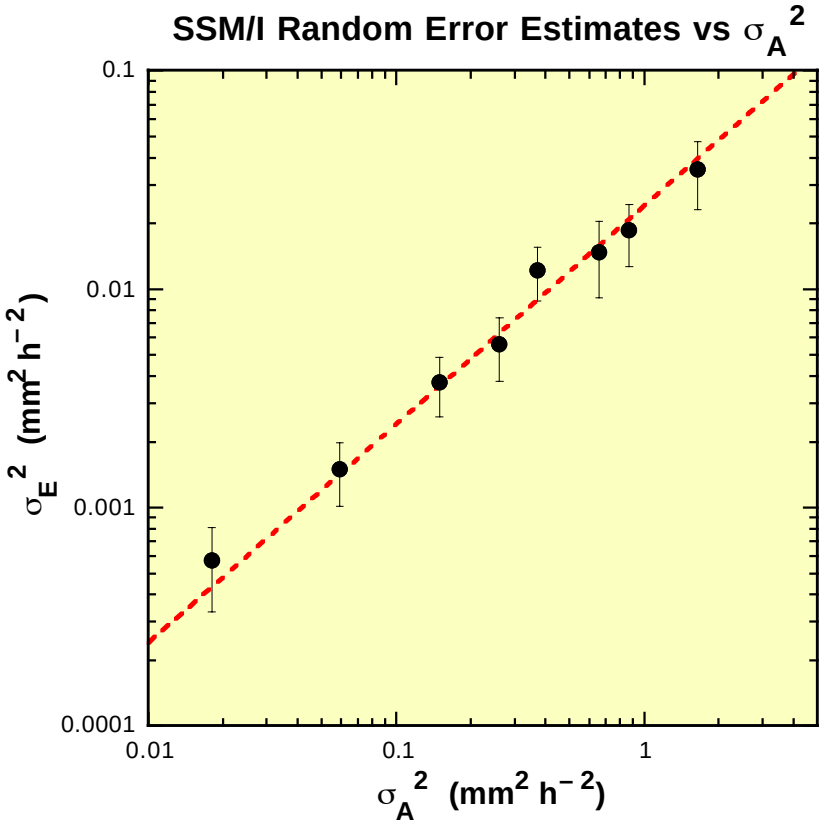

Figure 28. Estimates of the mean squared random error in monthly average rainfall obtained from microwave instruments aboard either of two Defense Department meteorological satellites, plotted versus the variance of area-averaged rain rate for 2.5° × 2.5° grid boxes. Their proportionality is predicted by a theory that allows us to estimate the amount of random error in gridded rainfall estimates such as those in Figure 27.

Thomas L. Bell, Code 913 (Thomas.L.Bell.1@gsfc.nasa.gov)

Effect of Radiative Cooling on the Relation between Cloud and Sea Surface Temperature

We have shown that one of the important processes in determining cloudiness over the pacific warm pool is radiative cooling in the surrounding subsiding atmosphere over the cold pool. Water vapor and clouds play an important role in maintaining the earth climate. Water vapor is recognized as a positive climate feedback process. This recognition is supported by observations that the area-mean greenhouse trapping of the clear-sky in the tropics generally increases from cold to warm sea surface temperature (SST). However, water vapor distribution is tightly coupled to clouds. Recent studies revealed that the change in the area of dry and subsiding regions relative to moist and convective regions determines the net greenhouse trapping. The local and remote processes determining the relative area are key climate issues.

In our work, we first examined the SST-cloud relationship in the tropical deep-convective regime and the surrounding subsidence regime in the Goddard Cumulus Ensemble model. Figure 29 schematically summarizes the overall model response in different low-boundary forcing conditions. Here the low-boundary forcing is expresses as SST contrast between the warm pool and cold pool (dSST). From weak to strong dSST, the area of downward motion increases while the magnitude of downward motion remains the same. This is because the strength of subsidence is limited by radiative cooling, which has a small variability. As a result, the area of radiatively

driven subsidence expands to produce an enhanced mass exchange between the warm pool and cold pool in response to enhanced dSST. The accompanying changes over the warm pool are a reduced convective area with an enhanced mean upward motion and rainrate.

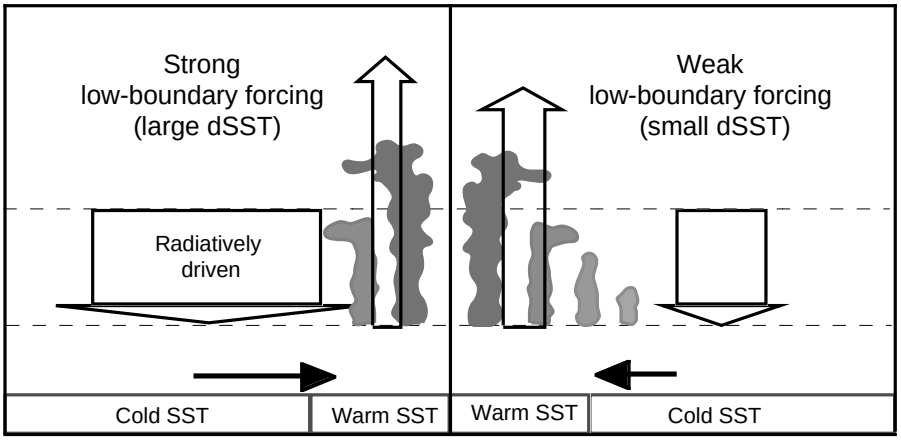

Figure 29. Schematic summary of tropical circulation and clouds in strong & weak low-boundary forcing regimes.

We then sought supporting evidence for the above model results by analyzing high cloud amount (A_{HC}) and vertical p-velocity (ω) as functions of SST. A_{HC} is derived from the International Satellite Cloud Climatology Project (ISCCP D2 data averaged to 2.5^ox2.5^o longitude-latitude spatial resolution and monthly time scale for the period of July 1983 - August 1994). Vertical p-velocity (ω) is derived from the NCEP reanalysis. The warm pool and cold pool within the tropical Pacific (20^oS-20^oN, 130^oE-110^oW) are separated by an isotherm so that the area of warm pool is 25% of the analysis domain. Mean cloudiness over the warm pool and cold pool are plotted in Figure 30a as a function of the corresponding dSST.

What did our analysis show? Over the warm pool, A_{HC} appears to be positively correlated with dSST for the weak low-boundary forcing condition (dSST<2.6^oC). This correlation is associated with the increased ascending (descending) motion over the warm (cold) pool with enhanced dSST as shown by the $-\omega$ at 500 hPa level in Figure 30b. The correlation is reversed for the strong low-boundary forcing condition (dSST>2.6^oC). The results suggest that the expanded subsidence area acts against increased clouds by enhanced upward mass flux over the warm pool. The subsidence produces less cloudy (more clear) regions over the warm pool when dSST is stronger than normal. Over the cold pool, A_{HC} and $-\omega$ are negatively correlated with dSST as is expected from the expansion of subsidence area with increasing dSST discussed above.

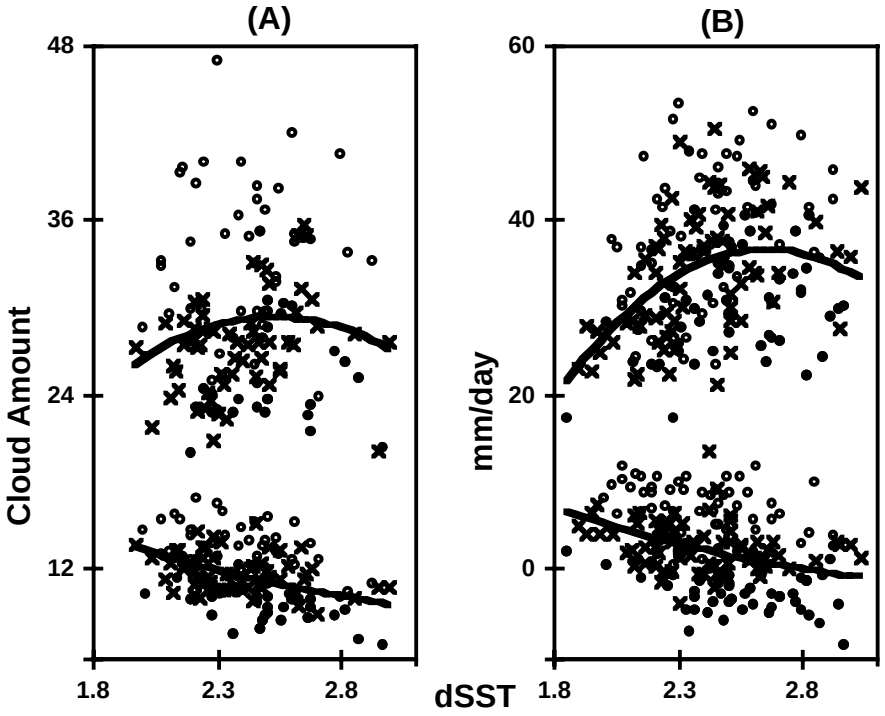

Figure 30. Scatter plot of A_{HC} (A), and -ω(500 hPa) (B) over the warm pool (upper) and cold pool (lower) as a function of dSST. o, x, and • correspond to the three categories of ω at 500 hPa: $(\omega-\omega_m)<-2$ mbday^{-1} (open circles), $|\omega-\omega_m|<2$ mbday^{-1} (crosses), and $(\omega-\omega_m)>2$ mbday^{-1} (close circles), where ω_m is the time mean ω.

The current analysis indicates that radiative cooling in the subsidence regime plays an important role in regulating SST-cloud interaction. The SST-cloud relation is crucial for understanding radiation-climate feedbacks in global climate change either induced naturally or anthropogenically.

Chung-Hsiung Sui, Code 913 (Chung-Hsiung.Sui.1@gsfc.nasa.gov)

The Use of Vegetation for Estimating Broken-Cloud Optical Properties from Surface Radiance Measurements

A key to predicting climate change is to observe and understand the global distribution of clouds and their physical properties such as optical thickness and droplet size. Since clouds change rapidly over short time and space intervals, they are difficult to simulate in computer models. But, it is essential that global climate models predict realistic spatial and temporal distribution of cloud optical depth. The best way to verify these distributions is to infer optical depth from global coverage satellite data. However, satellite methods have many sources of uncertainty; thus, independent and reliable ground-based estimates are essential for validation.

Although clouds vary substantially horizontally, all ground-based retrievals of cloud properties assume that clouds vary only vertically, ignoring not only horizontal in-cloud structure but also broken cloudiness. This assumption leads to misinterpretation of cloud properties and often makes their remote sensing impossible.

We developed a new technique that retrieves cloud optical thickness for broken clouds above green vegetation from surface measurements of zenith radiance in the visible (VIS) and near-IR (NIR) spectral regions. The idea of the method is simple. Since green vegetation reflects 40-50% of incoming radiation in the NIR and only 5-10% in the VIS region, ground measurements under thin clouds have little spectral contrast between VIS and NIR, while thick clouds reflect much more of the surface-reflected radiation in the NIR than in VIS. Based on this idea, we proposed to use a combination of measurements (spectral indices) in VIS and NIR to estimate cloud optical thickness.

Spectral indices that exploit this contrast are quite popular in the land-surface remote-sensing community. Among more than a dozen indices, the most widely used is the Normalized Difference Vegetation Index (NDVI) proposed by Jim Tucker from GSFC in 1979. By analogy with NDVI, we defined the Normalized Difference Cloud Index (NDCI) as a ratio between the difference and the sum of two radiances measured for two narrow spectral bands in VIS and NIR. NDCI uses the green vegetation as a powerful reflector illuminating horizontally inhomogeneous clouds from below. This provides the extra information needed to largely remove the ambiguity in measured radiance caused by radiative effects of the three-dimensional cloud structure. As a result, in contrast to conventional methods that yield almost entirely invalid results when clouds are broken, our new method gives a reliable estimate of the distribution of optical depth even for broken clouds.

For proof-of-concept measurements, we used downwelling flux at the surface measured by the Shortwave Spectrometer (SWS) at the Atmospheric Radiation Measurement (ARM) site in Oklahoma. SWS measures solar spectral flux between 0.35 and 2.5 μm, continuously, with spectral resolution 1 nm and temporal resolution of less than 1 minute. In addition to SWS, we also used the Microwave Water Radiometer (MWR) that measures column-integrated liquid water (LWP). Figure 31 shows a ratio between the difference and the sum of two downwelling fluxes (per unit incident flux) measured by SWS at 0.67 and 0.87 μm on April 29, 1998. Single and multilayered boundary layer clouds were reported that day. We plotted the ratio (flux NDCI) on the same plot as cloud LWP averaged over 1 minute. Clearly, flux NDCI is highly correlated with LWP. It is expected, though, that the correlation between NDCI and LWP will be even better if radiances are used instead of fluxes.

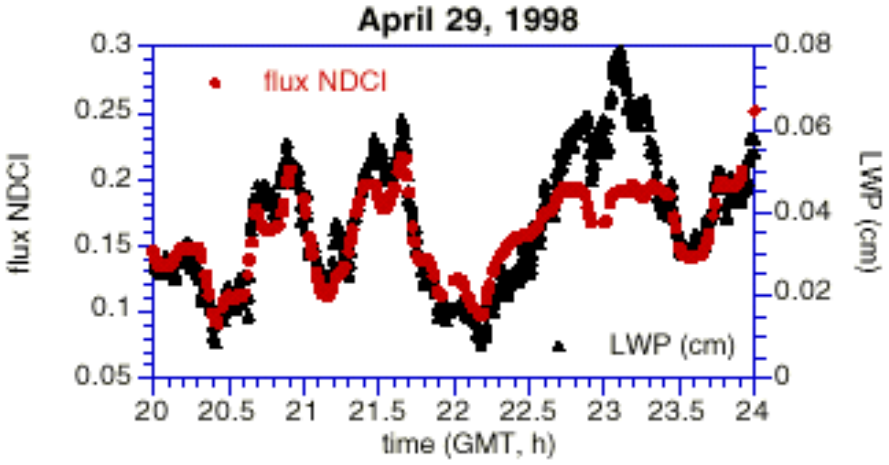

Figure 31. Flux NDCI and cloud LWP measured at the ARM site in Oklahoma and averaged in 1-minute increments. Note a poor correlation for about 40 minutes from 22.7 to 23.3 h. The reason for the poor correlation is not yet understood.

One of the proposed applications of the NDCI is developing a new "cloud mode" for the AERONET (AErosol RObotic NETwork) a ground based aerosol monitoring network that consists of identical multi-channel radiometers. As a product, the developed technique will yield the distribution of cloud optical depth at each AERONET site that is surrounded by green vegetation (more than 100 around the world). Global climate models can use the observations to produce realistic spatial and temporal distribution of cloud optical depth. The data will be added to the publicly available AERONET database.

The first preliminary results were reported in the Geophysical Research Letters: Marshak, A., Y. Knyazikhin, A. Davis, W. Wiscombe, and P. Pilewskie, 2000. Cloud-vegetation interaction: use of Normalized Difference Cloud Index for estimation of cloud optical thickness. Geophys. Res. Let., 27, 1695-1698.

Alexander Marshak, Code 913 (Alexander.Marshak.1@gsfc.nasa.gov)

Effects of Clouds on the Solar Heating of the Atmosphere in the Tropical Western Pacific

Do clouds enhance the solar heating of the atmosphere? Some studies using observed data have shown that clouds enhance the solar heating of atmosphere significantly, whereas radiative transfer models predict no excess heating due to the presence of clouds. Resolving this issue is very important because reliable climate model simulations and satellite remote sensing of the atmosphere depend crucially on accurate radiative transfer calculations. Nevertheless, this issue is still largely unresolved primarily due to the lack of comprehensive data sets for the radiation both at the top of the atmosphere and at the surface. To estimate the effect of clouds on the solar heating of the atmosphere, we need information on the clear- and cloudy-sky net downward solar fluxes at the top of the atmosphere and at the surface. Laboratory scientists have developed methodology to derive the surface solar radiation from measurements by the Japanese Geostationary Meteorological Satellite (GMS), which views the tropical western Pacific. The satellite-retrieved surface radiation is then combined with the CERES-retrieved top-of-the-atmosphere radiation to estimate the effect of clouds on atmospheric solar heating.

Table V shows that the magnitudes of atmospheric solar heating, Q, vary only slightly between the tropical western Pacific and South China Sea. It is ~102 W m-2 for the all-sky solar heating and ~80 W m-2 for the clear-sky solar heating. Thus, clouds enhance the atmospheric solar heating significantly by ~22 W m-2.

Table V. Solar Radiation Budget of the period January-August 1998.

	All-Sky	Clear-Sky	CRF
Tropical Western Pacific			
S_t	315	354	-39
S_s	215	276	-61
Q	100	78	22
South China Sea			
S_t	336	371	-35
S_s	233	289	-56
Q	103	82	21

CRF : Cloud radiative forcing
S_t : Net downward solar flux at top of atmosphere
S_s : Net downward solar flux at surface
Q : Atmospheric solar heating
Units: W m^{-2}

Ming-Dah Chou, Code 913 (Ming-Dah.Chou.1@gsfc.nasa.gov)

Climate Variability and Climate Change

A Multiyear Data Set of SSM/I-Derived Global Ocean Surface Turbulent Fluxes

The turbulent fluxes of momentum (or wind stress), latent heat of evaporation, and sensible heat at the global ocean surface are required for driving ocean models and validating coupled ocean-atmosphere global models. Laboratory scientists have developed methodology to retrieve a 7.5-year (July 1987-December 1994) data set of daily surface turbulent fluxes over global oceans from the Special Sensor Microwave/Imager (SSM/I) data and other data (Chou et al. 1995, 1997).

Accuracy of the retrieved surface air humidity (for computing latent heat fluxes) has been validated against the collocated radiosonde observations over the global oceans. The retrieved wind stress and latent heat flux show useful accuracy as verified against the research quality measurements of ship and buoy in the western equatorial Pacific (Chou et al. 1997, 2000). The 1988-94 seasonal-mean wind stress and latent heat flux show reasonable patterns related to seasonal variations of the atmospheric general circulation. The patterns of 1990-93 annual-mean turbulent fluxes and relevant parameters are generally in good agreement with those of a global analyzed flux data set that based on COADS (comprehensive ocean-atmosphere data set) with wind speed corrections. The retrieved wind speed is generally within ± 1 m s^{-1} of the modified COADS winds, but is weaker by ~1-2 m s^{-1} in the northern extratropical oceans. This discrepancy may be due mainly to higher modified COADS winds, which result from an underestimation of anemometer heights of ships. Compared to the COADS-based fields, the retrieved latent heat flux and sea-air humidity differences are generally larger, with significant differences in the trade wind zones and the oceans south of 40^oS (up to ~40-60 W m^{-2} and ~ 1-1.5 g kg^{-1}). The discrepancy is believed to be caused by higher COADS-based surface air humidity arising from the overestimation of dew point temperatures and from the extrapolation of observed high humidity southward into data-void regions south of 40^oS. The retrieved sensible heat flux is generally within ± 5 W m^{-2} of the COADS-based, except for some areas in the extratropical oceans, where the differences in wind speed have large impact on the difference in sensible heat flux. The data set of SSM/I-derived turbulent fluxes is useful for climate studies, forcing of ocean models, and validation of coupled ocean-atmosphere global models.

We have also combined the turbulent fluxes and the surface radiative fluxes retrieved from Japan's GMS data to study temporal and spatial variability of surface heat budgets and their relationship to sea surface temperature in the Pacific warm pool during the TOGA COARE (Chou et al. 2000). The impacts of Madden-Julian oscillations (intra-seasonal oscillations) and westerly wind bursts on the surface heat budget and sea surface temperature from November 1992 to February 1993 were included.

Shu-Hsien Chou, Code 912 (Shu-Hsien.Chou.1@gsfc.nasa.gov)

Planetary Sciences

Galileo Mission Highlights

Laboratory scientists were able to obtain for the first time an accurate measurement of the $^{14}N/^{15}N$ ratio on Jupiter using data from the Galileo Probe Mass Spectrometer (GPMS). The probe entered Jupiter's atmosphere in December 1995. These new results give the best estimate to date of the protosolar $^{14}N/^{15}N$ ratio. The measurement is important because the reservoirs of nitrogen in the solar system are poorly constrained and for lack of a better value the terrestrial atmospheric N_2 has commonly been adopted as the solar system value. This data can now provide constraints, for example, on models that study such physical processes as atmospheric escape. Such processes might produce substantially different values for this atmospheric ratio on the terrestrial planets Venus, Earth, and Mars.

Nitrogen isotope measurements are very difficult to obtain from the singly charged ratio of $^{14}NH_3^+/^{15}NH_3^+$ at 17 and 18 amu because the contribution of water to 18 amu cannot be independently constrained. The spectral overlap is illustrated in Figure 32. Thus the new measurement comes from a study of the doubly ionized ammonia (NH_3^{++}) signal throughout the course of the probe's descent into the Jovian atmosphere.

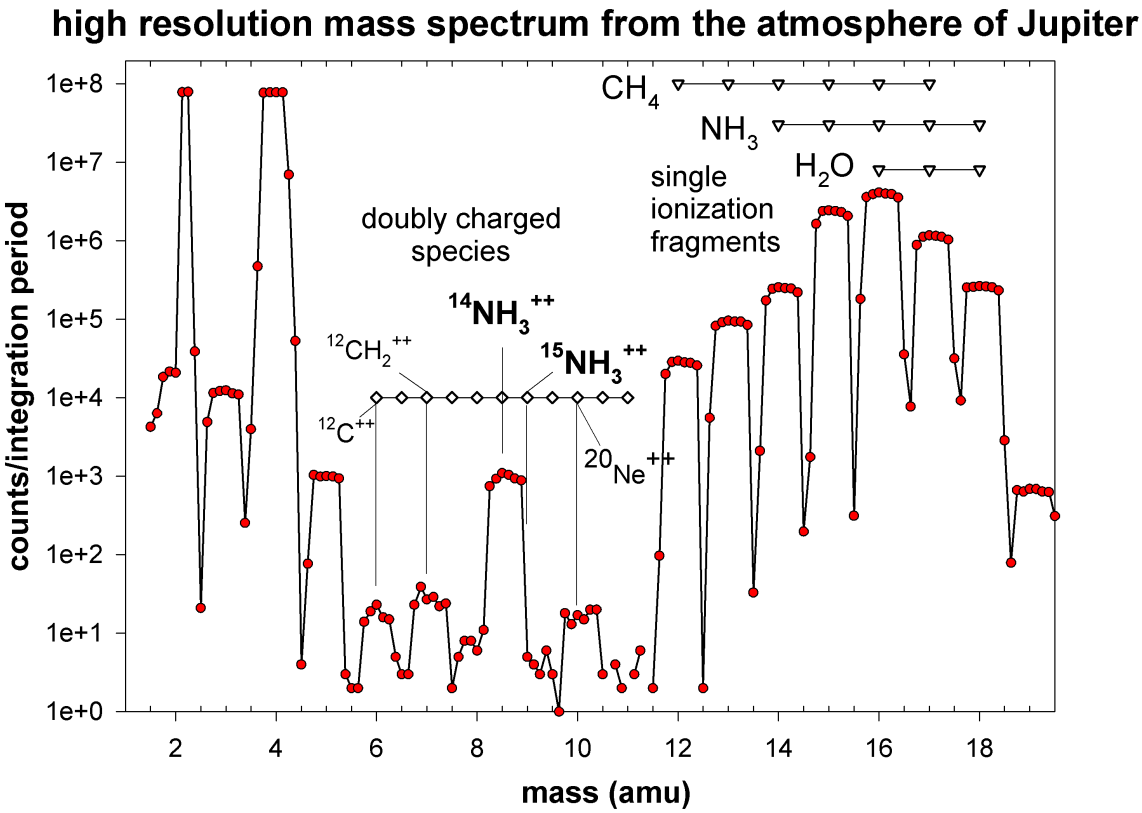

Figure 32. A 1/8 amu resolution mass scan obtained near the 17 bar pressure region of Jupiter's atmosphere shows the doubly charged species that are produced by electron impact ionization in the source of the mass spectrometer. The ratio of the doubly charged ammonia signal at 8.5 and 9.0 amu allows the Jovian and the protosolar $^{14}N/^{15}N$ ratio to be obtained. This ratio is considerably larger than the terrestrial ratio.

The isotope, $^{15}NH_3^{++}$ produces a signal at 9 amu while $^{14}NH_3^{++}$ produces a signal at 8.5 amu. The focus of the predetermined measurement sequence was on singly charged species and not on these doubly charged species. Hence, only one 8.5 amu measurement appears in this data set (at data step 5696) at a pressure of 17.2 bar. Nevertheless, we can predict the value of the 8.5 amu signal at any point in the probe descent. We do this by determining the ammonia fractional contribution to 17 amu and using the NH_3^+/NH_3^{++} ratio established from both the flight data itself and associated studies on the engineering unit presently operational in our laboratory. In one measurement period, the GPMS analyzed an enriched gas sample obtained from the Jovian atmosphere between 0.8 and 2.8 bar. The spectra from that sample give strong signals at 9 amu. It is from these measurement that we establish our best value of this ratio.

The Jovian and protosolar $^{14}N/^{15}N$ ratio established by these measurements is 430 with uncertainties of only a few percent. This ratio is consistent with several other recent observations such as the ISO (Infrared Space Observatory) measurement of Jovian ammonia and a very recent detailed study of solar wind implanted nitrogen in lunar samples. Our present result greatly reduces the uncertainty remaining from these studies. The ratio we measure at Jupiter is also consistent with our present understanding of the $^{14}N/^{15}N$ ratio in N_2 in the interstellar medium. The GPMS isotope ratio of 430 can be compared with the corresponding terrestrial value of this ratio in atmospheric N_2 of 273. It is likely that the source material for the Earth's atmosphere,

including external contributions from primitive bodies such as comets, did not reflect this average value. In addition, fractionation of nitrogen over the lifetime of the Earth's atmosphere may also contribute to this difference.

Paul R. Mahaffy, Code 915 (Paul.R.Mahaffy.1@gsfc.nasa.gov)

Modeling

Data Assimilation

Improving Four-Dimensional Global Data Sets and Short-Range Forecasts Using TRMM and SSM/I-Derived Rainfall and Moisture Observations

Laboratory for Atmospheres research has shown that assimilating rainfall and moisture observations derived from spaceborne passive microwave sensors in global models can significantly improve the quality of global data sets and short-range forecasts. Specifically, assimilation of rainfall and total precipitable water (TPW) data derived from TRMM Microwave Imager (TMI) and SSM/I improves not only the hydrological cycle but also key climate parameters in the tropics in the GEOS analysis.

Figure 33 shows the results of assimilating 6-hour averaged rainfall and TPW in the GEOS DAS for June 1998. The panels show the improvements on four assimilation fields: tropical precipitation, TPW, outgoing longwave radiation (OLR), and outgoing shortwave radiation (OSR). The monthly-mean spatial biases and error standard deviations are substantially reduced.

The apparent exceptions are biases in the tropical-mean precipitation and OLR. The slightly larger precipitation bias demonstrates that the rainfall assimilation algorithm is more effective in reducing than enhancing precipitation. The apparent increase in the OLR bias reflects the virtual elimination of the negative OLR bias associated with errors in precipitation. Eliminating the negative OLR bias leaves a tropical-mean bias dominated by the positive, but reduced, bias in the rain-free regions.

Overall, rainfall assimilation reduces the state-dependent systematic errors in clouds and radiation in raining regions, while TPW assimilation reduces errors in the moisture field to improve the longwave radiation in clear-sky regions. The OSR errors in the GEOS analysis are dominated by errors in clouds; the improved OSR indicates improved cloud patterns.

The improved analysis also leads to better short-range forecasts in the tropics, as shown in Figure 34. This work illustrates the potential of using space-based rainfall and TPW observations for improving numerical weather prediction and the quality of assimilated global data sets for climate research.

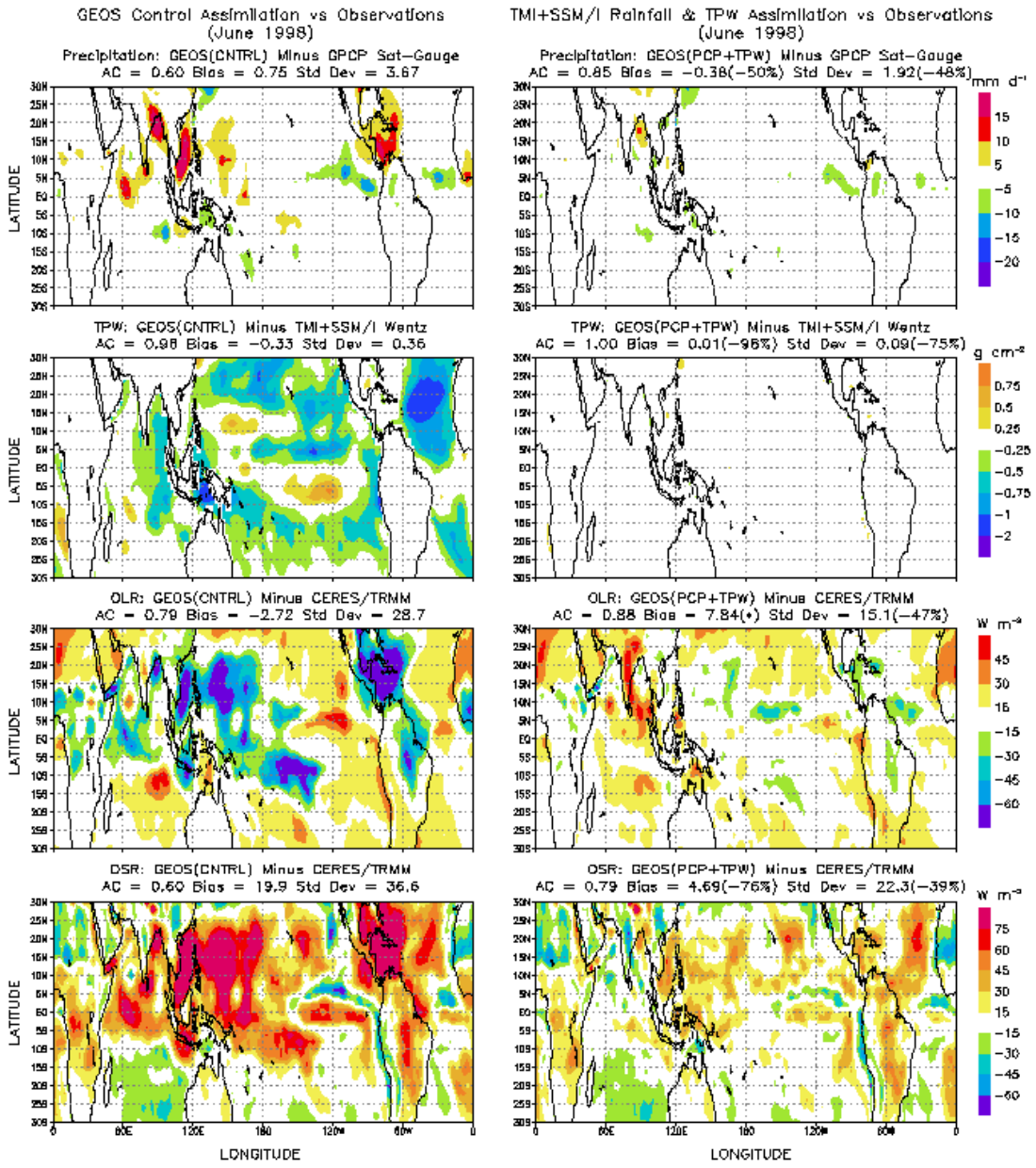

Figure 33. NASA GEOS assimilation results with and without TMI and SSM/I observations for June 1998. Left panels show errors in the monthly-mean tropical precipitation, total precipitable water, outgoing longwave radiation, and outgoing shortwave radiation in the GEOS control assimilation. Right panel shows the impact of assimilating TMI and SSM/I rainfall and TPW observations on these fields. Percentage changes relative to errors in the GEOS control are given in parentheses.

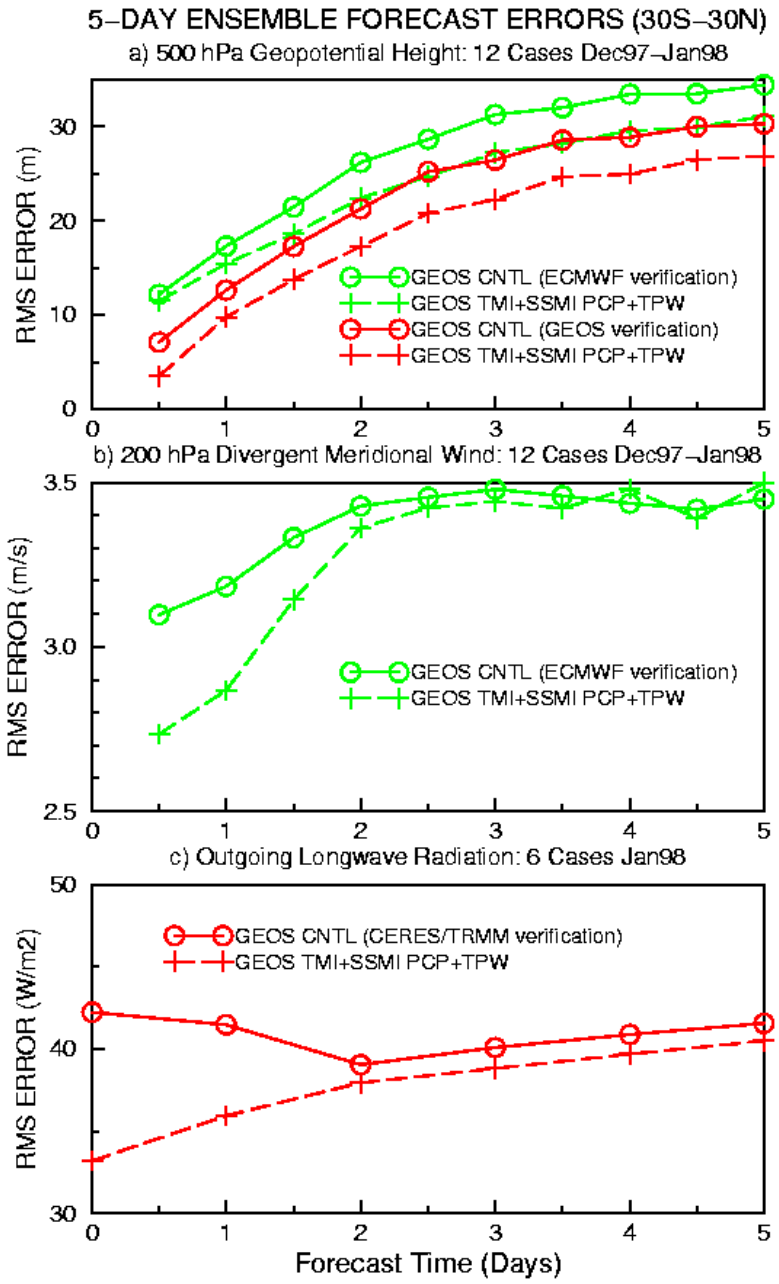

Figure 34. (a) Five-day ensemble forecast rms errors in tropical geopotential height at 500 hPa. Results in green are verified against the ECMWF analysis and results in red are verified against the average of the GEOS control analysis and the TMI and SSM/I rainfall and TPW assimilation. (b) Same as (a) except for the 200 hPa divergent meridional wind verified against the ECMWF analysis. (c) Same as (a) except for the OLR verified against CERES/TRMM observations.

Arthur Hou, Code 910.3 (Arthur.Y.Hou.1@gsfc.nasa.gov)

DAO Supports the SOLVE Mission

An important role for the DAO over the last decade has been supporting NASA's satellite validation missions and aircraft campaigns. The DAO continued this support while participating in the SAGE-III Ozone Loss and Validation Experiment (SOLVE). Several DAO scientists traveled to Kiruna in northern Sweden for several weeks between December 1999 and March 2000. There, they collaborated with the team of meteorologists and experimental physicists and chemists who used NASA's DC-8 and ER-2 aircraft to measure ozone and other important trace gases in and around the polar vortex.

Meteorological analyses and forecasts from the DAO and other centers were used in the field to help plan the flights. Medium-range forecasts were used to assess the prospects of flying inside the polar vortex or along the edge to measure several critically important trace gases and aerosols. One-day forecasts helped fine-tune the flight paths. The flight criteria were to be able to fly through cold regions while avoiding turbulence. Polar stratospheric clouds in these cold regions are sites of substantial chemical processing of air. DAO scientists collaborated with meteorologists from other centers to determine where these conditions were met.

Figure 35 shows a time series of DAO meteorological analyses and forecasts of 50-hPa geopotential height (red bundle of contours between 1962 and 1978gpdm) and temperature (shaded green and blue for values of less than 200K and 195K, respectively). The time (moving from left to right) extends from February 5 through February 10, 2000. The analyses (top row) show the transition from a triangular, cold polar vortex, which had dominated the flow since the latter third of January, to a warmer, elongated polar vortex, associated with a minor stratospheric warming. In the lower stratosphere, forecasting of such transitions is known to be difficult. Here, though, the DAO system captured the change in vortex structure. The 5-day forecast for February 10 shows a slightly large, cold vortex core, failing to capture the full magnitude of the warming event. However, the 4-day and shorter forecasts all show a reasonable structure (right-hand column).

The lessons learned were substantial. The DAO analyses and forecasts proved to be reliable products compared to those of other major centers. These products served as a validation for the GEOS-3 (Terra) system. The forecasts were generally of good quality, with a slight warm bias and a tendency to zonalize the stratospheric flow. The DAO analyses were used in interpreting Solve data, giving important input to chemical-transport models in the Atmospheric Chemistry and Dynamics Branch at GSFC.

DAO will continue to support such field campaigns. The next is Trace-P, a mission to study trace gases and aerosols in the western Pacific region. This mission will take place in the spring of 2001. In November 2001, DAO will support a field campaign based in Darwin, where ground-based (sonde, radar, and lidar) measurements will be used to study the excitation and propagation of internal gravity waves, which propagate from the troposphere to the mesosphere.

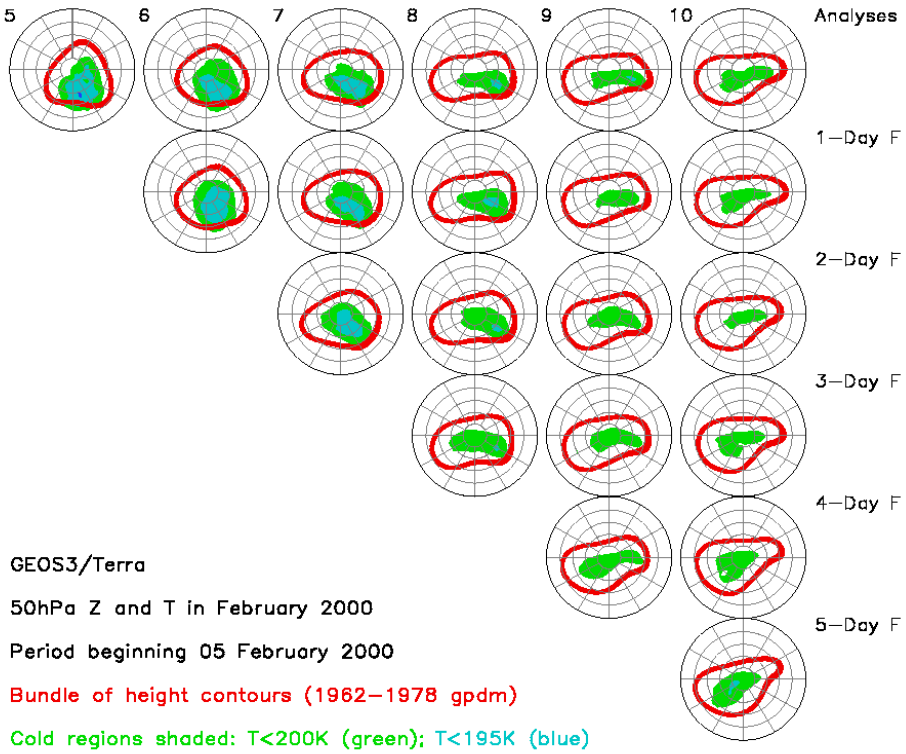

Figure 35. A time series of DAO meteorological analyses and forecasts of 50-hPa geopotential height (red bundle of contours between 1962 and 1978gpdm) and temperature (shaded green and blue for values of less than 200K and 195K, respectively).

Steve Pawson, Code 910.3 (spawson@dao.gsfc.nasa.gov)

The Predictability of Seasonal Means During Northern Summer

It is well established that, during northern winter, El Niño-related sea surface temperature (SST) anomalies in the tropical Pacific produce a strong atmospheric wave response emanating from the tropics into both hemispheres. Furthermore, a number of recent experiments in which ensembles of atmospheric general circulation model (AGCM) simulations are forced with observed SSTs, indicate that the signal-to-noise ratios in the atmospheric circulation are substantially greater than one over much of the Pacific North American region, and that this is primarily due to ENSO. In contrast, during northern summer, the wave response to the El Niño Southern Oscillation (ENSO) SST anomalies is much weaker, and the nature of the link between the tropical SST and extratropical climate is unclear.

We have here performed a large ensemble of seasonal hindcasts using the NASA Seasonal-to-Interannual Prediction Project (NSIPP-1) AGCM forced with observed SST and sea ice. We focused on the northern summer cases. These cases consisted of 9-member ensembles for each year for the period 1980-1999. Each hindcast began with observed atmospheric initial conditions (from NCEP/NCAR reanalyses) in mid-May and extended to the end of August. The nine members of each ensemble differed only in the atmospheric initial conditions (separated by 12 hours and centered on 00z May 15). The soil conditions were those obtained from a previous long AMIP-style integration. All results presented here represent June-July-August (JJA) means.

Figure 36 shows the first two empirical orthogonal functions of the JJA mean observed SST over the 20 years (1980-1999). Together these functions explain about 40% of the variance in the JJA SST distributed approximately equally between the two modes. The first mode shows warming (cooling) in the eastern Pacific and the Indian Ocean. The second mode has warming (cooling) in the central tropical Pacific and cooling (warming) in the extratropical western Pacific and the tropical and North Atlantic. Figure 37 shows the correlation of the ensemble mean height (the signal) with each of the SST modes. The first mode is primarily associated with enhanced (reduced) heights throughout the tropics when the tropical SST anomalies are warm (cold). The correlations are largest over the eastern tropical Pacific and the Indian Ocean, where EOF 1 has the largest amplitude. The strongest correlations are confined to the latitude band +/-30°. The second mode indicates a strong zonally symmetric extratropical response, with enhanced heights in the tropical Pacific and reduced heights throughout the middle latitude bands of both hemispheres. There is also an indication of a wave component emanating from the central tropical Pacific.

A further analysis of the AGCM's 200mb height hindcasts shows that a substantial fraction of the predictable component of the height is associated with those two SST modes. We are currently examining the link between these modes and precipitation variability over the summer continents.

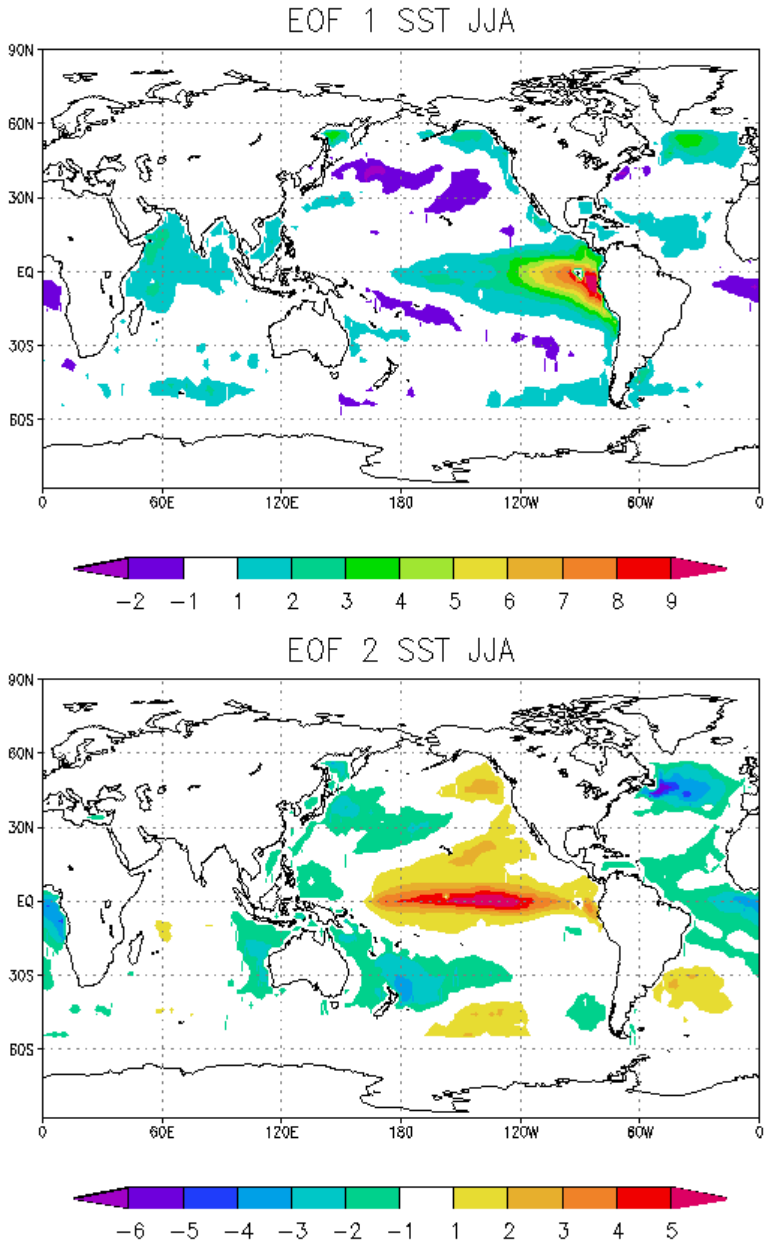

Figure 36. Top panel: First empirical orthogonal function (EOF) of sea surface temperature (SST) for June-July-August averages for 1980-1999. Bottom panel: Same as top panel except for the second EOF of SST.

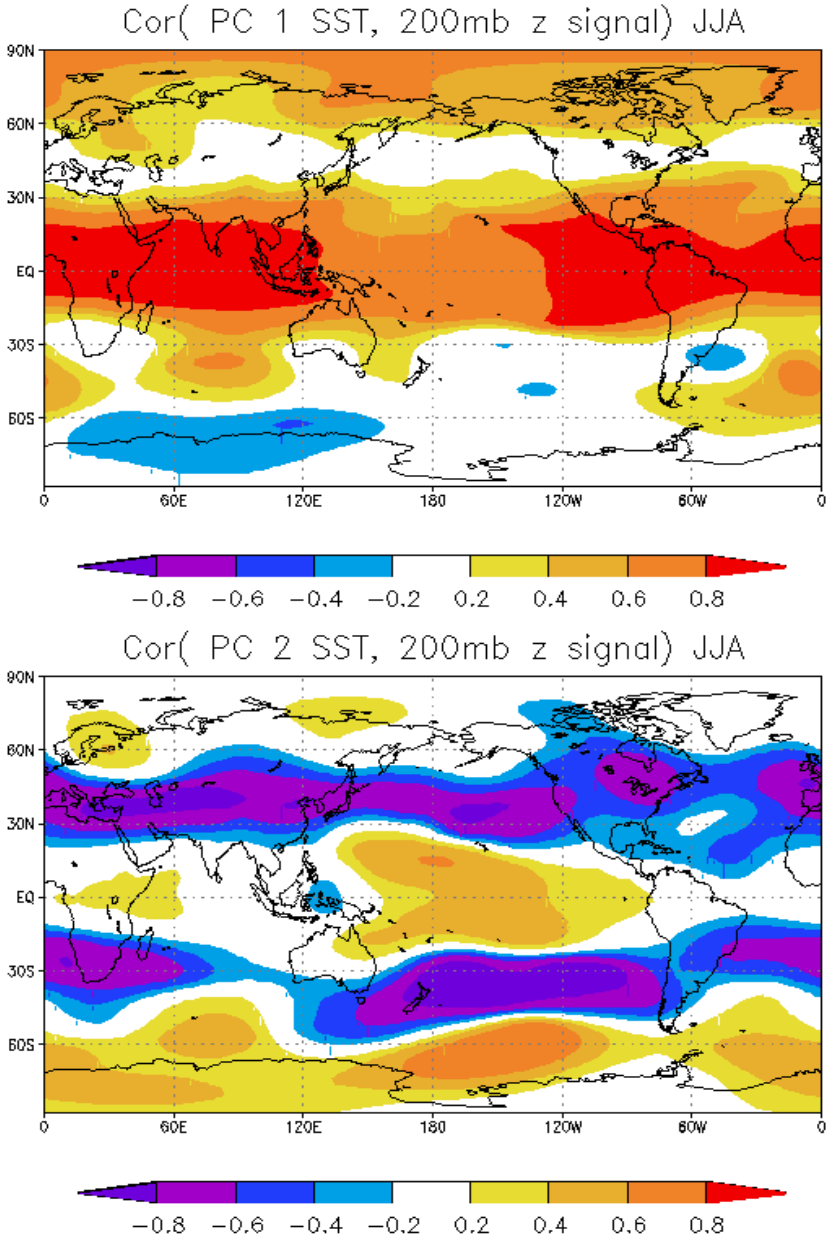

Figure 37. Top panel: Correlations between the first principal component (PC) of sea surface temperature (SST) and the AGCM ensemble mean 200mb height field at every grid point for June-July-August averages for 1980-1999. Bottom panel: Same as top panel except for the second PC of SST.

Siegfried Schubert, Code 910.3 (Siegfried.D.Schubert.1@gsfc.nasa.gov) and Max Suarez, Code 913

An Analysis of the Madden-Julian Oscillation

The Madden-Julian Oscillation (MJO) is a well-known and important component of tropical variability on intraseasonal time scales. The MJO is clearly seen in the upper tropospheric velocity potential field as an eastward-traveling zonal wave number one structure varying on time scales of 40 - 60 days. The MJO also manifests itself in a number of other fields. Perhaps most importantly, it has a dominant signature in large-scale tropical heating and precipitation variability. It thus plays an important role in the hydrological cycle of the tropics and subtropics (in particular the Asian summer monsoon). A number of studies suggest that the MJO also has a significant impact on the extratropics (for example in the southwestern United States), and that the MJO may enhance forecasts on weekly to monthly scales. On seasonal and longer scales, the MJO is primarily a source of noise superimposed on the slower components of the climate system. We don't yet know whether the rectified signal of the MJO (the "envelope" of noise) is predictable on time scales longer than individual MJO events, and whether the noise is important for proper simulation of the slower modes (e.g., ENSO) in coupled models.

The immediate goal of this project is to perform a systematic analysis of the MJO from observations and currently available long-term reanalysis data. The longer term goals are (1) to develop diagnostic tools to routinely assess the veracity of the MJO in general circulation model simulations and assimilated data, (2) to develop a better understanding of the predictability of the MJO, and (3) to assess the role of the MJO in ENSO.

The left panel of Figure 38 shows the MJO in terms of the first complex empirical orthogonal function (CEOF) of the 200mb velocity potential field based on the NCEP/NCAR reanalysis for the period 1979-1998. All fields shown here are filtered to retain only time scales between 20 and 90 days. The CEOFs are ideal for representing traveling waves and in this case we capture 3/4 of the variability in the velocity potential field in a single mode. The figure shows the evolution of the wave one mode over a complete cycle. The left panel is the same as the right, except for NOAA outgoing longwave radiation. This field also shows eastward propagation, but the signal is largely confined to the eastern hemisphere.

Figure 39 shows the time evolution of the real part of the first EOF of the velocity potential field (green line) and the rectified signal (red line). During some periods the MJO activity clearly lasts considerably longer than a single oscillation of the MJO. An extreme case is 1979 during which the MJO was active almost the entire year, and it went through about 7 cycles. Still other years the MJO is for the most part weak and poorly define (e.g. 1989). These results serve as the basis for an ongoing study of the structure, forcing and predictability of the MJO in observations and models on a wide range of time scales.

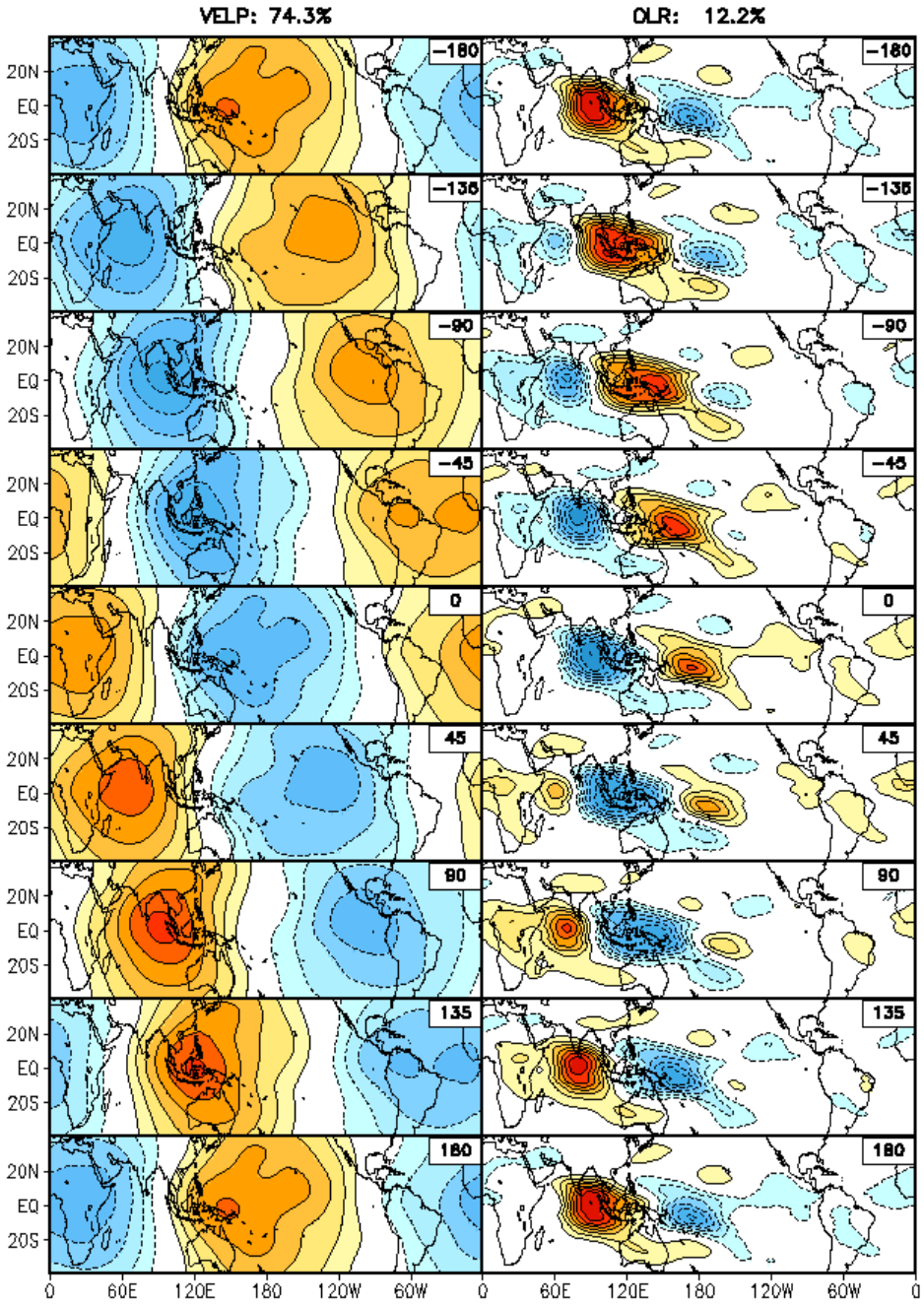

Figure 38. Left panel: One cycle of the first complex empirical orthogonal function (CEOF) of the 200mb velocity potential (20-90 day filter) based on NCEP/NCAR reanalysis data for 1979-1998. Right panel: Same as left panel except for NOAA OLR.

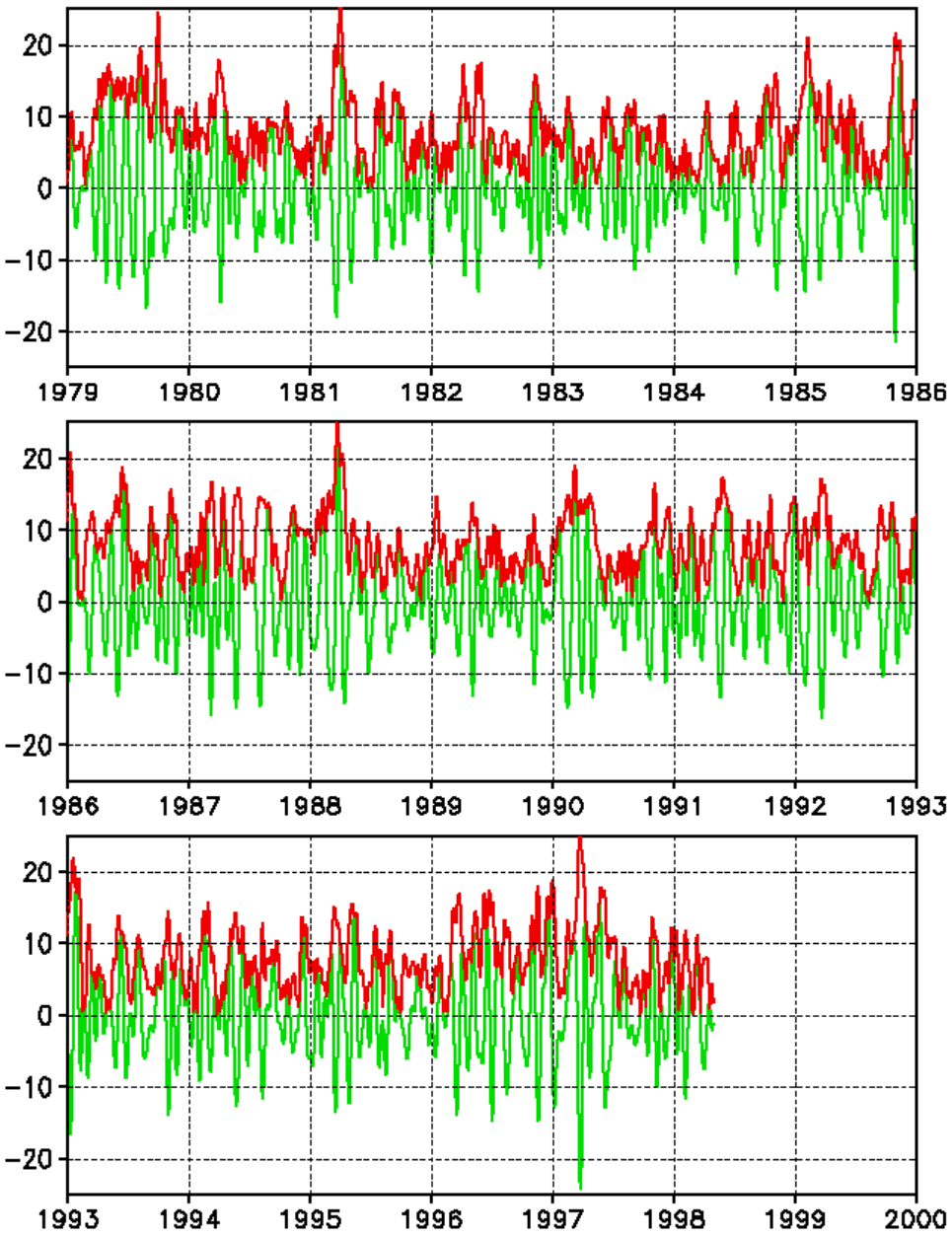

Figure 39. Time series of the modulus (red line) and real part (green line) of the first complex empirical orthogonal function (CEOF) of the 200mb velocity potential (20-90 day filter) based on NCEP/NCAR reanalysis data for 1979-1998

Siegfried Schubert and Yehui Chang, Code 910.3 (Siegfried.D.Schubert.1@gsfc.nasa.gov)

GEOS Ozone Data Assimilation System

The GEOS ozone data assimilation system became operational in January 2000. It has been running in near-real-time and providing global 3-dimensional ozone analysis fields in support of the instruments on the EOS Terra satellite. The ozone analysis fields are obtained by assimilation of the Total Ozone Mapping Spectrometer (TOMS) and the Solar Backscatter Ultra-Violet/2 (SBUV/2) instrument ozone observations into an ozone transport model.

The upper panel of Figure 40 shows an example of the total column ozone analysis produced by the system (i.e., integral of the ozone amount in a vertical column of the atmosphere, measured in Dobson units). The TOMS observations of total column ozone for the same day are shown in the lower panel of the figure with unobserved regions shaded in white. Although TOMS takes 24 hours to obtain the near-global coverage shown here, the analysis produced by the system is global and instantaneous. The analysis fills temporal and spatial gaps in TOMS observations: between the orbits in the tropics and in the unobserved polar night region in the northern high latitudes. The analyzed ozone agrees well with the input TOMS and SBUV observations. In addition, the transport model captures the dynamical variability in the ozone field. Comparisons with independent measurements have shown very good agreement of the ozone analysis profiles with independent profile measurements from the Halogen Occultation Experiment on board NASA's Upper Atmosphere Research Satellite.

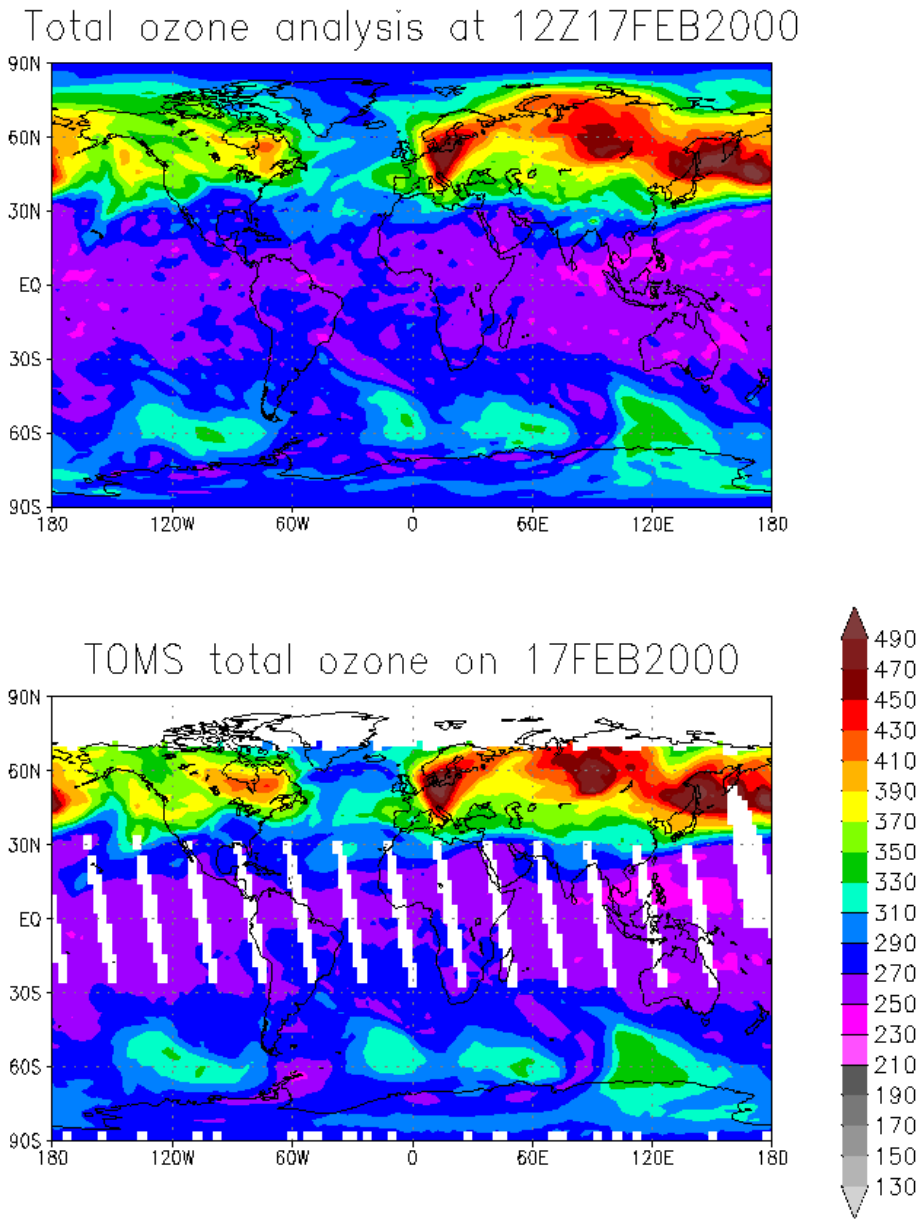

Figure 40. GEOS Ozone Data Assimilation.

Lars Peter Riishojgaard, Code 910.3 (larspr@dao.gsfc.nasa.gov)

Land Temperature Assimilation

The accurate representation of the land surface in weather and climate prediction models is critical, due to its partitioning and complex dynamic storage of water, energy, and carbon. Land surface temperature is a critical value for NASA instrument teams and Earth scientists, and it is one of the few land surface state variables readily observable from space. While land surface models have progressed significantly over the last two decades, error and bias of the land temperature can occur because of interactions with the atmospheric climate and meteorology (through clouds, radiation and precipitation) in addition to uncertainties in the land processes (specification and heterogeneity).

To better represent the land surface boundary in the DAO reanalysis system, we have developed a method to assimilate skin temperature into land models. Our development and testing has progressed through scientific collaboration between the Global Land Data Assimilation System (GLDAS) research group in the Hydrological Sciences Branch (Code 974) and the Data Assimilation Office (Code 910.3). A key finding of this work was that overcoming diurnal biases requires more than a traditional long-term bias correction. By extending the bias correction to compensate for long-term diurnal biases, we significantly improved the representation of the surface temperature. An effort is underway to integrate the skin temperature assimilation into the DAO reanalyses.

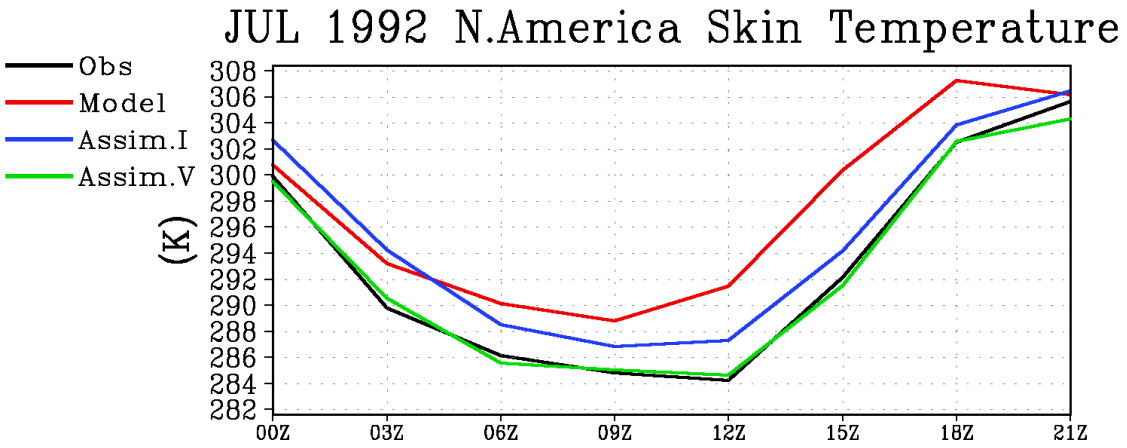

Figure 41. Monthly mean diurnal cycle area-averaged for the land points of central North America. ISLSCP Observations (Black), Model simulation (Red), Assimilation Experiment I (Blue) and Assimilation Experiment V (with incremental semi-diurnal bias correction) (Green). Note that in this case we are assimilating ISLSCP skin temperatures.

Arlindo da Silva, Code 910.3 (Arlindo.M.Dasilva.1@gsfc.nasa.gov) or Paul Houser, Code 974 (Paul.R.Houser.1@gsfc.nasa.gov)

Hurricanes

Numerical Modeling of Hurricanes

We employed a mesoscale numerical weather prediction model to simulate hurricanes, using high horizontal-grid resolution (1-4 km). Specifically, we simulated Hurricane Bob (1991) at a 4-km grid resolution to investigate the role of surface fluxes and vertical mixing in the boundary layer on storm intensity and structure.

We used four different boundary layer scenarios. Each scenario varied in its formulation of vertical mixing within the boundary and the surface fluxes. Our simulations revealed strong sensitivity of the precipitation structure and storm intensity, as measured by the surface pressure within the eye and by maximum wind speed within the eyewall. To isolate the separate effects of vertical mixing and surface fluxes, we performed some simulations using multiple surface flux schemes with a single vertical mixing scheme and others using multiple vertical mixing schemes with a single surface flux scheme. These experiments indicated that simulated intensity is determined largely by the surface fluxes rather than by the vertical mixing. There was one exception. In that simulation, excessively deep vertical mixing acted to dry the lower boundary layer and reduce hurricane intensity.

A 1.3-km grid scale simulation of the same storm provided unprecedented detail of the kinematic, thermodynamic, and cloud microphysical structures within the storm. Our analysis of heat and momentum budgets for this storm suggests an important role of horizontal eddy heat and momentum transports into the eye. These transports act to intensify the warm core and increase winds inside the eyewall. Our findings agree with theoretical predictions using vortex Rossby wave concepts and vortex instability analyses. In collaboration with researchers at Colorado State University, we are analyzing this simulation to study the evolution of vortex Rossby waves and their relationship to storm intensification and precipitation structure.

Hurricane modeling is often difficult because large-scale analyses seldom include an adequate representation of the hurricane vortex. Often, we must insert a "bogus" vortex to represent the initial hurricane structure. This bogus vortex is generally an oversimplification of the existing storm and can result in forecast errors associated with adjusting the model to initial imbalances. We have devised a method for creating a bogus vortex that uses 4-dimensional variational data assimilation to minimize initial imbalances.

We applied this method to hurricanes observed during the NASA Convection and Moisture Experiment (CAMEX-3) in 1998. The methodology involves assimilation, over a short time period, of bogus surface pressure and wind distributions that reflect observed conditions and the horizontal scale of the vortex. During the assimilation period, the velocity and mass fields are adjusted so that they coincide with the specified surface pressure and wind distributions and the dynamical equations of the model. We applied this technique to Hurricane Georges, which occurred during CAMEX-3, prior to its landfall in Puerto Rico. In our simulation, we used a 36-km grid for the assimilation of the bogus vortex and a 12-km grid for the forecast. Our results (Figure 42) show a dramatic improvement of the intensity and rainfall forecast compared to a simulation without the bogus vortex.

We also successfully applied the bogus vortex technique to the case of Hurricane Bonnie (1998). In this case, the forecast was conducted using a 4-km grid scale to better resolve the cloud microphysical processes and details of the storm structure. Validation of the model against observations is essential for identifying shortcomings of the model physics that contribute to forecast errors and making improvements to the model. We are validating our simulated precipitation structure against TRMM precipitation radar reflectivity data and CAMEX-3 aircraft data. Our comparison to TRMM (Figure 43) suggests that the model is successful in capturing the observed asymmetry of the precipitation field. However, the model tends to produce reflectivities that are too large and a distribution of rain that is more convective and less stratiform than that observed by TRMM. The differences between simulated and observed rainfall help us improve the model cloud microphysics.

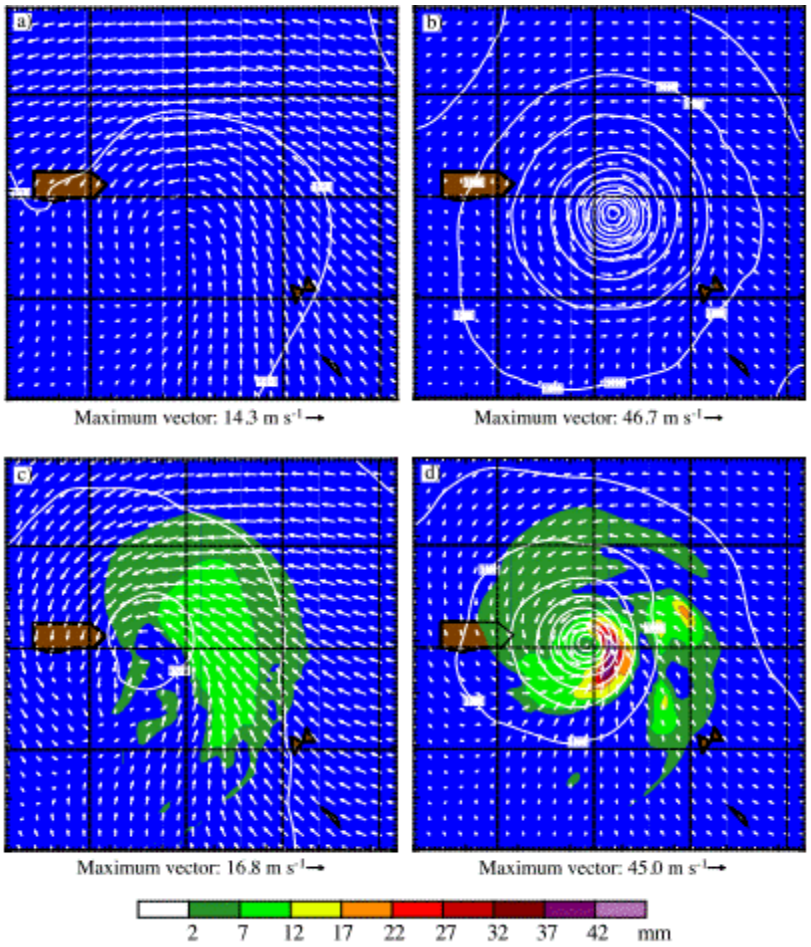

Figure 42. Panels demonstrate the impact of assimilation of a bogus hurricane vortex into the model initial conditions for a simulation of Hurricane Georges (September 1998). Upper panels show initial sea-level pressure (contours at 4 mb intervals) and 850 mb wind vectors for simulations (a) without a bogus vortex and (b) with a bogus vortex. Hurricane Georges at this time was a major hurricane just east of Puerto Rico. The storm is poorly defined in the large-scale analysis used to generate the model initial conditions in (a). Inclusion of the bogus vortex substantially improves the initial storm structure in the model. Lower panels show the 6 hour forecasts of sea level pressure, 850 mb winds, and 6 hour accumulated precipitation for the simulations (c) without and (d) with the bogus vortex. Substantial improvement of the precipitation forecast is obtained with the bogus vortex.

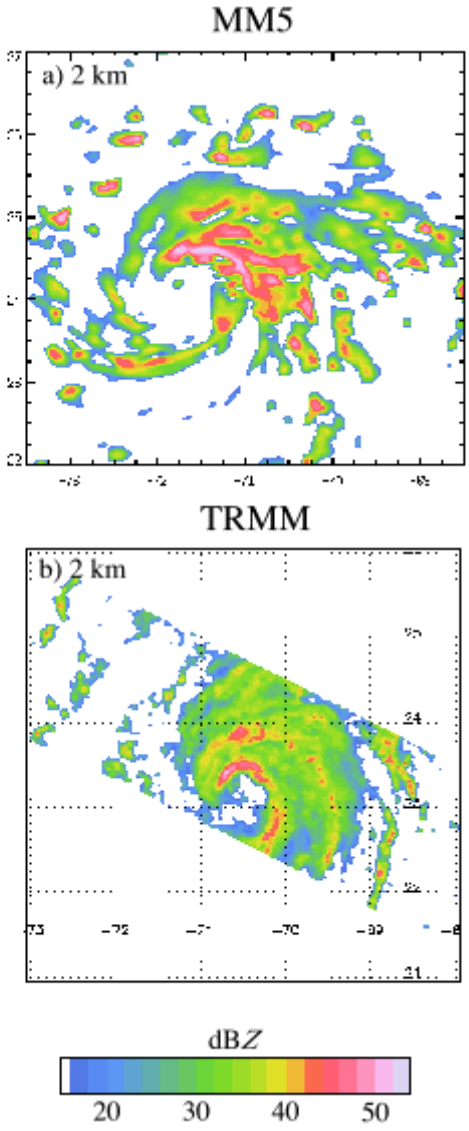

Figure 43. Comparison of MM5 simulated radar reflectivity (a) and TRMM precipitation radar reflectivity (b) at 2 km above mean sea level. For both panels, the display area is 5º latitude by 5º longitude and the color table is identical. The model captures the asymmetry of the rainfall pattern, with most of the rainfall to the north and east of the center.

Scott Braun, Code 912 (Scott.A.Braun.1@gsfc.nasa.gov)

Physical Processes

Force-Restore Snow Physics in SSiB

Laboratory staff designed a model to remedy systematic weaknesses in the snow processes of Simple SiB (SSiB). The new model separates the snow-pack from land so as to allow the snow-pack to have its own temperature and energy-exchange processes (Figure 44, left diagram). This snow physics led to better snow-melt and melt-water recharge timings.

We introduced a force-restore snow-layer atop the rest of the snow pack (Figure 44, right diagram) to further reduce the remaining time delay in the simulated snowmelt (as derived from systematic investigations of snowmelt and melt-water discharge for the Russian Wheat Belt region using GSWP ISLSCP Initiative I data sets). The force-restore snow-layer now produces better diurnal amplitude of snow-surface temperatures while attenuating the surface solar-flux more realistically. It also generates some mid-winter snowmelt during the warm spells, enabling the snow accumulation to agree better with observations. Thus, the revised snow-model not only improves the remaining delay in the snowmelt (varying from 1-4 weeks), but is also accompanied by several overall improvements of the hydrologic processes that are central to land-atmosphere interactions.

In previous work, we described (a) inaccuracies in the satellite retrievals of snow under dense forest canopies, (b) assumptions in modeling, and (c) possible cold bias of the ISLSCP surface air temperature data. Nevertheless, we now show significant improvements in the snow-accumulation/snow-melt simulation in response to improved snow-physics.

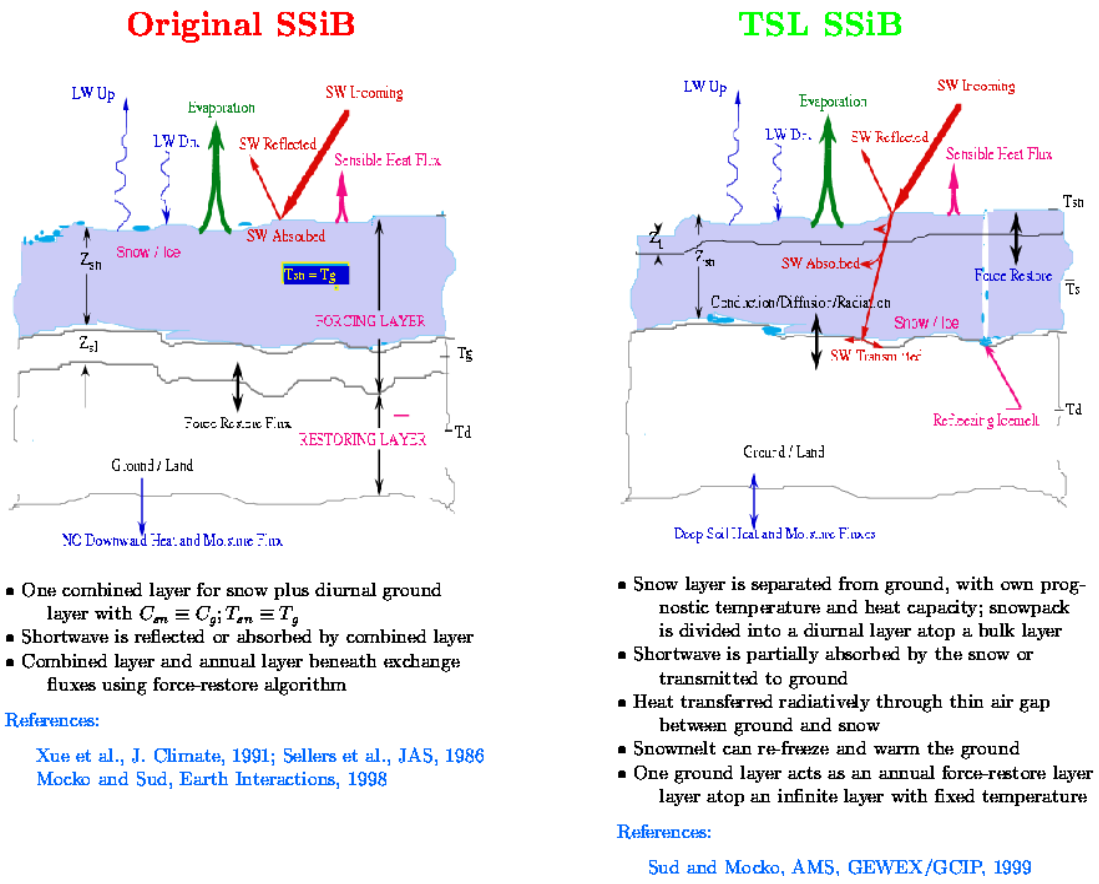

Figure 44. New snow-physics model development.

Yogesh Sud and David Mocko, Code 913 (Yogesh.C.Sud.1@gsfc.nasa.gov)

Cirrus Cloud Models

Laboratory staff completed a primary analysis of results from the GCSS WG2 Idealized Cirrus Model Comparison Project. The 17 models participating in this project represent the state of the art. They range in complexity from very high resolution 3-dimensional (3-D) large eddy simulation (LES) models, to 3-D and 2-D cloud resolving models (CRMs), to single column model (SCM) GCMs. The microphysical, and radiative, components are similarly varied, ranging from simple relative humidity (bulk) schemes to fully size-resolved (bin) treatments of microphysical growth and development.

A key finding is that significant scatter exists in the results from the various state-of-the-art models for each of the idealized cases that were simulated. These cases included "warm" and "cold" cirrus forming in a neutrally stratified, versus stably stratified, supersaturated layer (RHI = 120%) under nighttime conditions (infrared radiative processes only versus no radiation) subject to relatively weak forcing (imposed cooling equivalent to adiabatic ascent at 3 cm s^{-1}). In the "warm" cirrus case, differences of up to a factor of 2 were found in horizontally averaged, vertically integrated ice water path (IWP). These differences appear even among the "built-for-cirrus" cloud-resolving models (CRMs) after 4 hours of development/forcing. This is the least detailed measure of model result. Differences grew appreciably in the subsequent decay phase when the forcing was turned off. Moreover, even greater differences arose in the "cold" cirrus case. Results from "heritage" CRMs were somewhat more divergent. (“Heritage” CRMs were models originally built to simulate deep convection or boundary layer clouds.) Results from the SCMs spanned the range of CRM results. These results characterize the current state of knowledge on cirrus cloud processes, indicating that significant uncertainties exist with resultant implications for large-scale climate models where cirrus cloud radiative effects play an important role.

A second major finding is that the results of the bulk "built-for-cirrus" models diverge systematically and substantially from those of the bin models. This is especially true for cold cirrus and even for gross parameters such as horizontally averaged, vertically integrated ice water path (IWP). Smaller, more numerous ice crystals in the bin model simulations of cold cirrus would account for the substantially greater ice water path and internal circulation intensity, and the smaller effective ice water fall speeds. (Ice water fall speed was an independent parameter in some bulk models but required bin-by-bin calculation in bin models.) The same explanation holds for significant differences in gross cloud geometry (upward growth of cloud top versus relatively static cloud top in bulk model simulations, Starr et al., 2000). These results strongly focus the science issues needing observational confirmation. The results also provide new insights into how this confirmation might be accomplished, even with the present observational limitations and uncertainties.

This work was a key topic of an international workshop (Joint GCSS Working Group on Cirrus Cloud Systems with the GCSS Working Group on Extratropical Layer Cloud Systems) and was presented to special GEWEX session of Spring 2000 AGU meeting and as lead paper at the 13th International Conference on Clouds and Precipitation in August 2000.

David Starr, Code 912 (David.O.Starr.1@gsfc.nasa.gov)